AN INVESTIGATION OF ELBOW JOINT INCONGRUENCY IN DOGS USING RECONSTRUCTED COMPUTED TOMOGRAPHY

By

Toby J Gemmill BVSc CertSAS MRCVS

Dissertation submitted for the Degree of Master of Veterinary Medicine

University of Glasgow

Division of Companion Animal Sciences
Institute of Comparative Medicine
University of Glasgow Veterinary School
Glasgow

May 2005

SUMMARY

In part one of this project, the use of reconstructed computed tomography (rCT) for the investigation of elbow joint surface incongruency was validated using 12 cadaver elbows. Following gross clinical and radiographic examinations which excluded any obvious elbow pathology, the elbows were scanned in pairs in the same computed tomography (CT) scanner. From these scans, standardised frontal and sagittal plane images were reconstructed using medical image analysis software (Omnipro, California, USA). From the reconstructions, humeroradial (HR) and humerulnar (HU) joint spaces were measured from both frontal (giving FrHR and FrHU values) and sagittal (giving SagHR and SagHU values) plane images.

Firstly, four elbows were scanned on three occasions to assess the effects of specimen positioning and CT acquisition on rCT images (inter-image variation). A single observer reviewed the scans and recorded the HR and HU values. These values from the different scans were then compared graphically and using a Pearson test. The data indicated good inter-image agreement ($0.77<R<0.80$).

Secondly, intra-observer variation was assessed using scans from four elbows. A single observer reviewed the scans on three occasions and recorded the HR and HU values. The values on the three occasions were then compared graphically and using a Pearson test. The data indicated good intra-observer agreement ($0.77<R<0.92$).

Thirdly, inter-observer variation was assessed, again using scans from four elbows. As before, standardised HR and HU values were recorded and compared graphically and using a Pearson test. The data indicated moderate inter-observer correlation (R=0.47) though graphical analysis indicated low inter-observer variation.

Fourthly, the ability of rCT to accurately image the elbow joint surface anatomy was assessed. Four elbows were scanned and frontal plane rCT images created. FrHR and FrHU values were recorded. The elbows were frozen at -20^0 centigrade and then sectioned in the frontal plane with a band saw. FrHR and FrHU values were measured from the frozen sections. A further four elbows were then scanned and sagittal plane rCT images created. SagHR and SagHU values were recorded. These elbows were also frozen and then sectioned in the sagittal plane. SagHR and SagHU measurements were recorded from the frozen sections. As well as direct visual comparison of the rCT images and frozen sections, corresponding FrHR, FrHU, SagHR and SagHU values from the rCT and frozen sections were compared graphically and using a Pearson test. Visually, the rCT images appeared to accurately reflect the frozen section anatomy. Joint space values exhibited good agreement (R=0.88), confirming rCT can accurately image joint surfaces and allow joint spaces to be measured.

Finally, four elbows were studied to assess the ability of rCT to image known elbow joint surface incongruencies. Elbow joint incongruencies were created by radial shortening using an external skeletal fixator. Incremental 1mm incongruencies were induced, up to a maximum of 4mm. The elbows were scanned after each shortening. FrHR and SagHR values were recorded.

FrHU values were also recorded. From frontal plane images, joint incongruency (JIFr) was calculated by subtracting FrHU values from FrHR values. In addition, a direct measurement was made of radioulnar joint incongruency (JIRU) from sagittal plane images. These values (FrHR, SagHR, JIFr and JIRU) were then compared with the known incongruencies using graphical techniques. The data indicated that FrHR and SagHR correlate well with known incongruencies, indicating that rCT can be used to accurately measure changes in joint spaces in both the frontal and sagittal planes. JIFr also correlated well with known incongruencies, but JIRU correlated poorly. This indicates that frontal plane images can be used to accurately measure joint incongruency, but that direct JIRU measurements are unreliable.

In part two of this project, a retrospective study was undertaken to evaluate elbow joint congruency in dogs suffering coronoid process disease. Based on clinical, radiographic and transverse CT examinations, elbows were divided into control or coronoid disease (CD) groups. Standardised rCT images were formatted in the frontal and sagittal planes. HR and HU measurements were obtained from the images and incongruencies calculated by comparing the two measurements.

42 CD and 29 control elbows were identified. No incongruencies were noted at the coronoid base. At the level of the coronoid apex, CD elbows exhibited a significant radioulnar incongruency compared to controls ($p<0.0001$). Comparing CD and control elbows at the level of the apex, the HR joint space was increased in CD elbows ($p=0.0006$) whereas no difference was noted in the HU space.

Part two of this study supports the hypothesis that joint incongruency is associated with coronoid disease in dogs. However, the precise mechanism of development of this incongruency could not be determined from the data.

Table of Contents

DECLARATION

I, Toby Jonathon Gemmill, do hereby declare that the work in this dissertation is original, was carried out by myself, and has not been presented for the award of a degree at any other university.

Signed:

Mr Toby J Gemmill BVSc CertSAS MRCVS

Date:

Acknowledgments

I would like to thank Gawain Hammond for assistance with radiography and collection of CT scans for the cadaver phase of this project. I would also like to thank Alan **Purves** for assistance with sectioning of the frozen cadaver specimens.

I would like to thank Nicola Milne and Victoria Johnson for assisting with the collection of radiographs and the CT scans for the clinical phase of the project, and for assistance with the use of Omnipro software.

I would like to thank Dr Dom Mellor for assistance with statistical analyses.

I would also like to express my gratitude to all those who have provided other advice and support, including Dylan Clements, Stephen Clarke, Mike Farrell and Professor Martin Sullivan, and my supervisors Professors David Bennett and Stuart Carmichael.

Finally I would like to acknowledge BSAVA Petsavers who generously provided the funding for part one of the project.

Table of Figures

Abbreviations

CA	California
CD	coronoid disease
Cm	centimetre
CrCd	craniocaudal
CT	computed tomography
Dx	diagnosis
GH	Mr Gawain Hammond MRCVS
GUVS	University of Glasgow Veterinary School
FCP	fragmented coronoid process
Fr	frontal
FrA	frontal plane rCT image at the level of the coronoid apex
FrB	frontal plane rCT image at the level of the coronoid base
FrHR	humeroradial joint space measured from frontal plane images
FrHU	humeroulnar joint space measured from frontal plane images
HR	humeroradial
HU	humeroulnar
iFrFR	increase in FrHR
iFrHU	increase in FrFU
iSagHR	increase in SagHR
iSagHU	increase in SagHU
IOHC	incomplete ossification of the humeral condyle
JI	joint incongruency
JIFr	joint incongruency measured on frontal plane reconstruction
JIRU	joint incongruency estimated from direct radioulnar measurement

JISag	joint incongruency measured on sagittal plane reconstruction
Kg	kilogram
LAC	long axis of the medial coronoid process
MM	millimetre
MRI	magnetic resonance imaging
NAD	nothing abnormal diagnosed
OCD	osteochondrosis dissecans
rCT	reconstructed computed tomography
RU	radioulnar
Sag	sagittal
SagB	sagittal plane rCT image at the level of the coronoid base
SagHR	humeroradial joint space measured from sagittal plane images
SagHU	humeroulnar joint space measured from sagittal plane images
TJG	Mr Toby Gemmill MRCVS
UAP	ununited anconeal process
UK	United Kingdom
USA	United States of America

Introduction and Literature Review

Elbow dysplasia, or abnormal development of the elbow joint, is a common condition in dogs (Morgan and others 1999). The term was originally used to describe a generalised arthrosis of the joint with or without an ununited anconeal process (Corley and Carlson 1965). However, the definition of this syndrome has changed considerably as our understanding of the condition has improved. Currently, elbow dysplasia is commonly taken to represent a group of conditions affecting the developing elbow joint including fragmented medial coronoid process (FCP), ostechondrosis or osteochondritis dissecans of the medial aspect of the humeral condyle (OCD) and ununited anconeal process (UAP) (Shultz and Krotscheck 2003). Other authors have included less common elbow joint abnormalities such as ununited medial epicondyle (Walker 1998, Meyer-Lindenberg and others 2004a).

FCP is the most common of these conditions (Van Ryssen and Van Bree 1997) and can occur alone or less commonly in conjunction with OCD (Bennett and others 1981, Guthrie and Pidduck 1990, Meyer-Lindenberg and others 2002a) or UAP (Meyer-Lindenberg and others 2002b, Rovesti and others 2002). FCP appears to be over-represented in certain breeds such as Labrador Retrievers, Golden Retrievers, Rottweilers and Bernese Mountain dogs (Morgan and others 2000) and is the most common cause of forelimb lameness in juvenile dogs (Olsson 1975, Grøndalen 1976, Grøndalen 1979, Bojrab 1981). Male dogs are affected more commonly than females (Huibregste and others 1994). Because of its high prevalence in working and guide dogs, the condition has important financial as well as welfare implications.

FCP is characterised by fissuring and fragmentation of the cartilage and bone over the craniolateral aspect of the medial coronoid process. Osteochondral fragments may remain in situ, or may separate from the base of the coronoid process and become displaced (Grøndalen and Grøndalen 1981). Cartilaginous 'kissing lesions' of the medial aspect of the humeral condyle and secondary osteoarthritis are also commonly seen (Grøndalen and Grøndalen 1981, Van Ryssen and Van Bree 1997). It has also been noted that cartilage erosion over the medial coronoid process and the medial aspect of the humeral condyle can occur in the absence of discrete bony coronoid fragmentation (Wind 1986b, Read and others 1990, Van Ryssen and Van Bree 1997, Schulz and Krotscheck 2003, Meyer-Lindenberg and Heinen 2004b). It is probable that FCP represents a specific lesion within a wider spectrum of pathology affecting the coronoid process and medial compartment of the elbow joint which can be termed 'coronoid disease' (CD).

Traditional treatment for CD has included both conservative and surgical management. Conservative management has been aimed at relieving the clinical signs associated with the condition and managing secondary osteoarthritis. Strategies have included exercise moderation (Read 1987), weight control (Kealy and others 2000), use of non steroidal anti-inflammatory drugs and steroid medications (Read 1987), physical therapy (Conzemius 2004), and the use of slow acting 'disease modifying' agents such as glucosamine, chondroitin, polysulphated glycosaminoglycans and pentosan polysulphate (Bouck and others 1995). Surgical treatment has traditionally consisted of fragment excision, either by open arthrotomy (Denny and Gibbs 1980, Bennett and others 1981, Read 1987, Read and others 1990) or arthroscopy (Bardet 1997, Meyer-Lindenberg and others 2002a). However, the results of surgical management have been disappointing, with many authors noting that radiographic degenerative changes tend to progress irrespective of treatment (Bennett and others 1981, Huibregste and others 1994, Theyse and others 2000). Some authors have described an improved outcome in surgically treated patients when compared to those treated conservatively (Henry 1984, Reid and others 1990) but other studies have not demonstrated this improvement (Huibregste and others 1994, Bouck and others 1995) and overall the benefits of surgery have been marginal at best. These poor results have led some authors to question the benefits of surgical retrieval of fragments (Bennett and others 1981), and have prompted further investigations into the pathogenesis of the disease.

Various factors have been identified as contributing to the aetiology of CD including genetics (Guthrie and Pidduck 1990, Maki and others 2000, Maki and others 2002), exercise, and nutrition (Grøndalen 1982). However, the precise pathophysiology is poorly understood. One study of 13 cadaver elbows by anatomic dissection and evaluation of elbow joint surfaces using light and scanning electron microscopy showed that the coronoid process does not develop from a separate centre of ossification to the remainder of the proximal ulna (Guthrie and others 1992a). This study indicated that early reports of 'ununited coronoid process' (Olsson 1974, Tirgari 1974, Tirgari 1980) were inappropriate. The lesions were thought to represent a form of osteochondrosis (Bennett and others 1981, Olsson 1983). The medial coronoid process ossifies between 12 and 22 weeks (Hare 1961) and may be susceptible to osteochondrosis during this period. Histological studies, however, have failed to support this view and are more suggestive of an osteochondral fracture of the medial coronoid process. Guthrie and others (1992b) evaluated osteochondral fragments which had been surgically retrieved from 24 dogs with FCP. No microscopic evidence of osteochondrosis was found, and the histological picture was more consistent with a fibrous non-union. Histologically confirmed osteochondrosis of the medial humeral condyle was identified in a further 25 dogs in the same study. Following treatment of clinical cases of FCP by subtotal coronoidectomy, Fitzpatrick and Reuter (2004) were able to evaluate both the loose fragments from the cranial aspect of the medial coronoid process, and the caudal base of the coronoid process from where the fragments had originated. Again, no histological evidence of osteochondrosis was found at the level of the medial coronoid process and the authors concluded that FCP was most likely the result of a non-healed osteochondral fracture.

Interestingly, in contrast to CD cases, two adult dogs suffering traumatic coronoid process fracture which were treated by fragment excision appeared to have minimal progression of osteoarthritis, suggesting that the fracture seen with CD is part of a more complex aetiology (Yovich and Read 1994). Decreased levels of type X collagen in the cartilage of affected coronoid processes have been noted (Crouch and others 2000) but the implications of this finding were unclear. It has been suggested that affected dogs may be predisposed to fracture due to metabolic or vascular anomalies of the coronoid process (Schulz KS 2004, personal communication) or due to abnormalities in the anatomy of the radial incisure of the ulna and the annular ligament (Robbins G 2004, personal communication), but there is little published evidence to support these theories.

It has been proposed that a developmental incongruency of elbow joint surfaces leads to disproportionate load bearing through the medial compartment of the joint (Wind 1982), and this could lead to subsequent development of cartilage lesions and coronoid process fracture (Hak and others 1998). An experimental study demonstrated that increased loading of portions of an articular surface following fracture mal-reduction can cause osteochondral fragmentation (Llinas and others 1999). One report highlighted that in Bernese Mountain dogs elbow joint incongruency and FCP are often concurrent findings (Ubbink and others 1999).

Wind (1986a) suggested that under-development of the trochlear notch of the ulna could result in increased load bearing at the anconeus and the medial coronoid process. Incongruency was noted in nine dogs suffering CD. The author suggested that the radius of curvature of the ulnar trochlear notch was decreased with respect to the radius of curvature of the humeral condyle. This discrepancy could lead to a trochlear notch which was too small to accommodate the humeral condyle, which could in turn lead to increased loading of the anconeal and coronoid processes and the development of classical lesions. A further radiographic study by the same author (Wind 1986b) demonstrated an increase in the relative size of the proximal ulna in breeds affected by elbow dysplasia. The author concluded this was due to the need for a larger trochlear notch to accommodate the humeral condyle, and that a failure of development of the trochlear notch could lead to the proposed incongruency. From a radiographic study using digital image analysis, Collins and others (2001) demonstrated a decreased arc of curvature of the cranial aspect of the medial coronoid process of Rottweilers, a breed commonly affected by CD, when compared with greyhounds, a breed not predisposed to CD. Another radiographic study comparing the trochlear notch of Bernese Mountain dogs with that of Rhodesian Ridgebacks came to a similar conclusion (Viehmann and others 1999) suggesting that the concept of humeroulnar incongruency may be a critical factor in the pathogenesis of the disease. However, other studies have indicated that bicentric concave humeroulnar incongruency may be a normal finding in both humans and dogs (Eckstein and others 1994, Preston and others 2000). Furthermore, osteoabsorptometry and joint contact area studies in normal elbows have indicated that the coronoid process may bear more load than the remainder of the semilunar notch (Maierl and others 2000). This work supports the theory of a physiological humeroulnar incongruency in normal dogs.

A second proposal is that relative undergrowth of the radius with respect to the ulna may lead to the development of a step defect between the proximal articular surfaces of the radius and ulna (Wind 1982, Morgan and others 2000), specifically between the radial head and the coronoid process. This theory is supported by cadaveric studies demonstrating an increase in loading of the medial coronoid process during radial shortening (Preston and others 2001) and by clinical information documenting the presence of coronoid fractures in dogs suffering radial shortening secondary to premature closure of the radial physes (MacPherson and others 1992). However despite this research, precise characterisation of incongruency in clinical CD cases has not been reported.

Based on these proposals, various osteotomies have been suggested as potential treatments for underlying incongruency. Three papers (Thompson and Robbins 1995, Bardet and Bureau 1996, Ness 1998) have described a proximal ulnar osteotomy, the rationale being that the osteotomy allows slight shortening and rotation of the proximal ulna which relieves abnormal loading on the medial coronoid process. It has also been demonstrated in cadavers that a shortening osteotomy of the ulna stabilised with an intramedullary pin can correct an incongruency previously induced by radial shortening (Preston and others 2001). Hulse (2002) described a radial lengthening osteotomy which also aimed to relieve abnormal loading of the medial coronoid process by proximal elevation of the radial head. However, these procedures can be associated with postoperative morbidity (Beale 2001, Meyer-Lindenberg and others 2001) and the theory of incongruency on which they are based is not fully established. Furthermore, it has been suggested that in affected elbows progressive collapse of the medial joint space may occur in the longer term (Schulz 2003). The mechanism of this collapse was proposed to have similarities to human unicompartmental knee osteoarthritis, in which an initial small decrease in joint space due to cartilage atrophy leads to increased weight bearing through the diseased portion of the joint. This then subsequently leads to further cartilage loss and accelerating joint space collapse (Rees and others 2001, Cameron and others 1997, Nagel and others 1996). If medial joint collapse does occur in diseased canine elbows, radial lengthening or ulna shortening osteotomies may actually increase loading of the medial compartment of the joint in the long term, which may worsen the outcome. A further retrospective case series of 83 dogs affected by CD (Fitzpatrick and O'Riordan 2004) suggested an aggressive intra-articular sub-total coronoidectomy may be beneficial for dogs suffering CD. The authors suggested this may relieve abnormal humeroulnar loading through the medial aspect of the elbow. However, despite superficially encouraging results, the series was uncontrolled and the data must be interpreted with caution.

Diagnosis of elbow joint inconguency can be challenging. Plain radiographs have been shown to be unreliable for the detection of elbow incongruency (Murphy and others 1998, Mason and others 2002). Arthroscopy can allow identification of incongruency (Beale 2002, Fitzpatrick and O'Rioran 2004), although the reliability of the technique has been questioned, since the introduction of the arthroscope into the elbow may induce or disguise the presence of incongruency in some cases. Furthermore, the technique is inherently invasive, limiting its usefulness as a screening tool. Plain and contrast-enhanced magnetic resonance imaging (MRI) have been used to image canine elbows (Snaps and others 1997, Snaps and others 1998, Snaps and others 1999), but the expense of MRI has limited its widespread application. Furthermore, bone resolution with MRI is inferior compared to computed tomography (CT). CT has become well established as a diagnostic tool for the investigation of elbow pathology in both humans (Franklin and others 1988, Holland and others 1994, Weber and Morrey 1999, Potter 2000, Edelson and others 2001) and dogs (Reichle and others 2000, Rovesti and others 2002). CT is especially useful for the investigation of canine coronoid process disease (Braden and others 1994, Korbel and others 2001, Rovesti and others 2002, Ring and others 2002) and has been shown to be more reliable than many other imaging modalities (Carpenter and others 1993, Gielen and van Bree 2003). Displaced fragments can also be easily identified (Korbel and others 2001). Occasionally, smaller non-displaced fragments may not be identified due to partial volume artefacts (Hathcock and Stickle 1993) though this is uncommon.

Some forms of elbow incongruency can be identified on transverse CT images. Boulay (1998) described an increase in the humeroulnar joint space at the centre of the trochlear notch in one affected elbow. However, the sensitivity and specificity of the technique was not evaluated.

After collection of transverse CT scans, sagittal and frontal plane reconstructed images can be created using a computer. These reconstructed images allow good visualisation of elbow joint surfaces (Reichle and others 2000, de Rycke and others 2002, Holsworth and other 2003). In human elbows, it has been shown that joint spaces can be reliably imaged (Seiler and others 1995). Direct measurement of radioulnar incongruency from reconstructed CT (rCT) images in canine elbows is possible, but the technique can be subjective and requires the use of geometric image analysis to diminish errors (Holsworth and others 2003). The reliability and accuracy of rCT for imaging of the canine elbow joint has not yet been fully established.

In part one of this study, we firstly aimed to define the rCT anatomy of the canine elbow and to assess the accuracy and reliability of rCT for the measurement of elbow joint spaces. Secondarily, we aimed to investigate the feasibility of rCT for the detection and measurement of elbow joint incongruency. Finally, in part two of the study, a cohort of dogs was evaluated to assess the joint surface congruency of control elbows and elbows affected with CD using rCT.

Materials and Methods

Part One – Cadaver Study

(i) Collection of cadaver elbows and storage

Twelve forelimbs were collected after shoulder disarticulation from cadavers which had been recently euthanased for reasons unrelated to the study. The cadavers were mixed breed collie-type dogs ranging from approximately 15 to 40 kg. The elbows of these forelimbs were subjected to a clinical examination to exclude any obvious abnormalities and to ensure a normal range of motion. The forelimbs were then wrapped in saline soaked towels and stored at -20^0 centigrade until the time of testing.

Prior to the imaging stage of the project, the limbs were thawed for 24 hours at room temperature. The saline soaked towels were left in place for this period. Immediately prior to imaging, the towels were removed and the limbs labelled with plastic tags to allow consistent identification.

At the end of the study the elbows were dissected and the articular cartilage inspected to confirm an absence of pre-existing pathology.

(ii) Radiography

Each elbow was radiographed using the same x-ray machine (Genius Vision HF, Villa Sistemi Medicali, Italy), a rare earth cassette (Quanta detail, Du

Pont, France) and high detail film (Cronex 10T, Agfar, UK). Exposure settings were adjusted depending on the tissue thickness of each elbow, measured with manual callipers. Tabletop exposures were performed without the use of a grid.

Neutral or slightly extended mediolateral, flexed mediolateral, and extended craniocaudal views were obtained for each elbow All films were developed using an automated processor (Cronex CX-130, Du Pont, France). The radiographs were examined for evidence of degenerative joint disease, and for evidence of gross joint surface incongruency. Any elbows showing pathology were excluded from the study.

(iii) Collection of computed tomography images

The elbows were scanned in pairs with the same CT scanner (Exel 2400 elite, Elscint Ltd, Haifa, Israel). Elbows were positioned side by side in slight extension using radiolucent foam wedges. The region to be scanned was identified using an initial craniocaudal survey view and included the entire elbow articulation from the anconeus to the radioulnar articulation distal to the coronoid process (Figure 1). Transverse CT slices were then collected using an automated program. Slice thickness was 1.2 mm with a bed increment of 1.0 mm. Approximately 30 transverse slices were required to image the elbow joint in this fashion. The scans were examined and any elbows showing pathology were excluded from the study. The scans were then archived using standard software (Omnipro Medical Software, CA, USA).

Figure 1 Craniocaudal survey view of the elbow joint. Area A is the region to be scanned

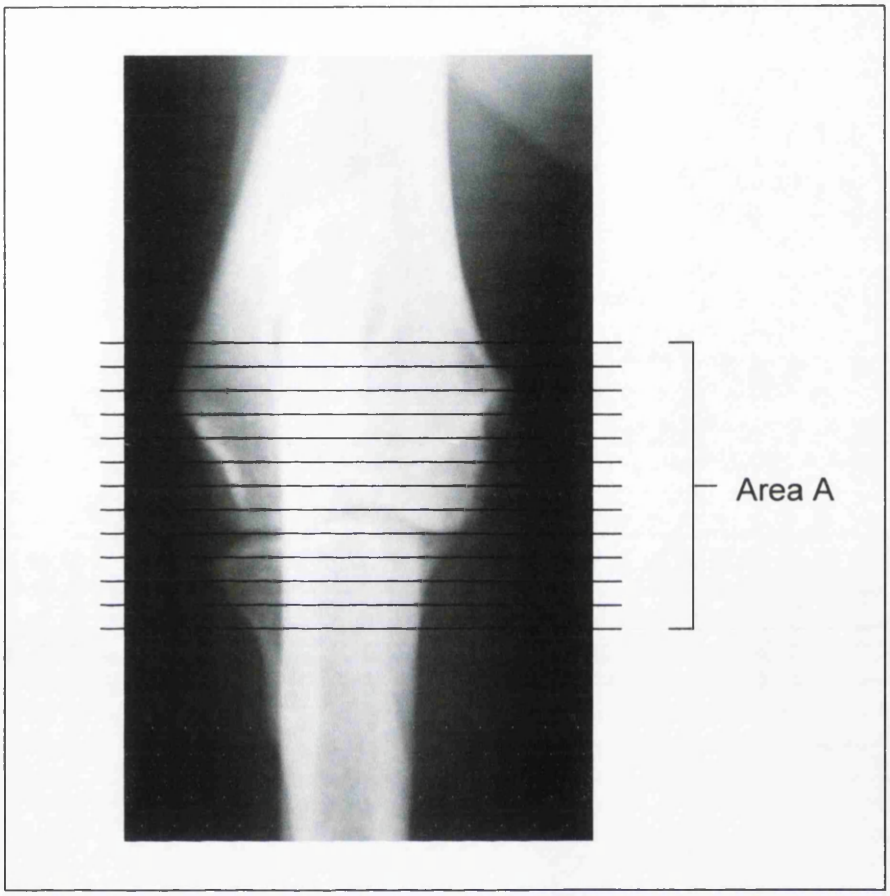

(iv) Creation of incongruency models and collection of images

Four elbows were selected for creation of a model of radioulnar incongruency (elbows 1, 7, 9 and 10). Two 3.5 mm cortical bone screws (Synthes, UK) were placed distally between the radius and the ulna, immediately proximal to the carpus. These screws prevented relative movement of the distal radius and ulna during subsequent testing. Through a medial approach (Piermattei and Johnson 2004) four 2.7 mm pilot holes were drilled through the radius in the mediolateral plane using a twist-type drill bit. 3.0 mm smooth pins (Veterinary

Instrumentation, Sheffield, UK) were placed through these predrilled holes and connected using linear motors and threaded connecting bars (Figure 2).

Figure 2 Cadaver specimen with ESF pins and linear motors applied. Two 3.5 mm screws can be seen distally, preventing relative movement between the distal radius and ulna. A mid diaphyseal radial ostectomy has been performed.

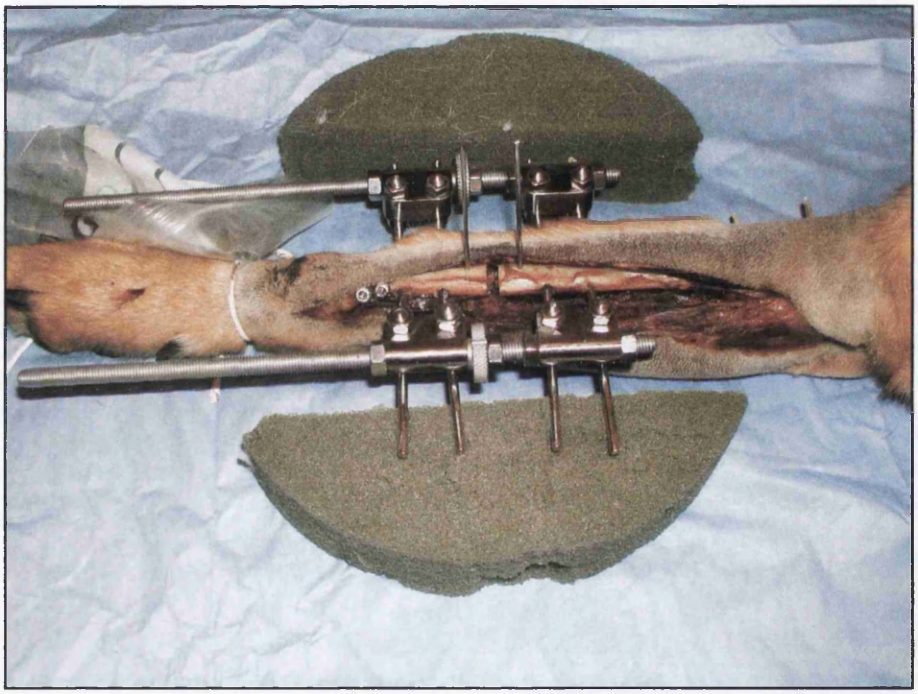

After locking of the linear motors, a 1 cm mid radial ostectomy was performed using an oscillating saw (Mini driver, 3M, UK). 1.6 mm Kirschner wires (Veterinary Instrumentation, Sheffield, UK) were then placed into the radius either side of the ostectomy in the craniocaudal plane. These wires were placed in a monocortical fashion and penetrated only the dorsal cortex of the radius. The wires were cut to 3 cm lengths (Figure 3). These wires acted as markers so as to allow accurate measurement of the relative movement between the proximal and distal radial fragments. Care was taken to ensure the apparatus was positioned so no superimposition of metal would occur during collection of CT scans of the elbow.

Figure 3 Marker wires placed in the dorsal aspect of the radius to allow accurate measurement of radial shortening. The ESF apparatus and radial ostectomy can also be seen.

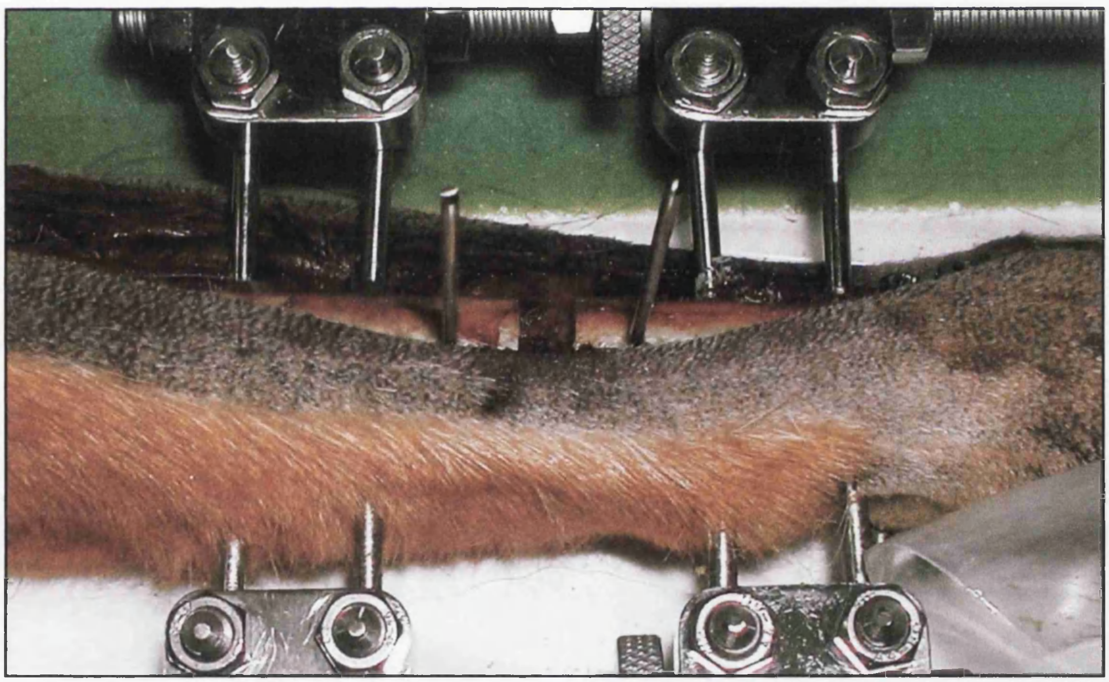

Finally, the interosseus, annular and lateral collateral (humeroradial) ligaments were sectioned using a scalpel blade. Further bone tunnels were drilled in the lateral aspect of the humeral condyle and the radial head using a 1.5 mm drill bit. Radiolucent wooden rods were placed in these tunnels to act as markers for accurate measurement of the relative movement between the humeral condyle and the proximal radius (Figure 4).

Figure 4 Radiolucent markers placed in the humeral condyle and radial head to allow accurate measurement of changes in the humeroradial joint space

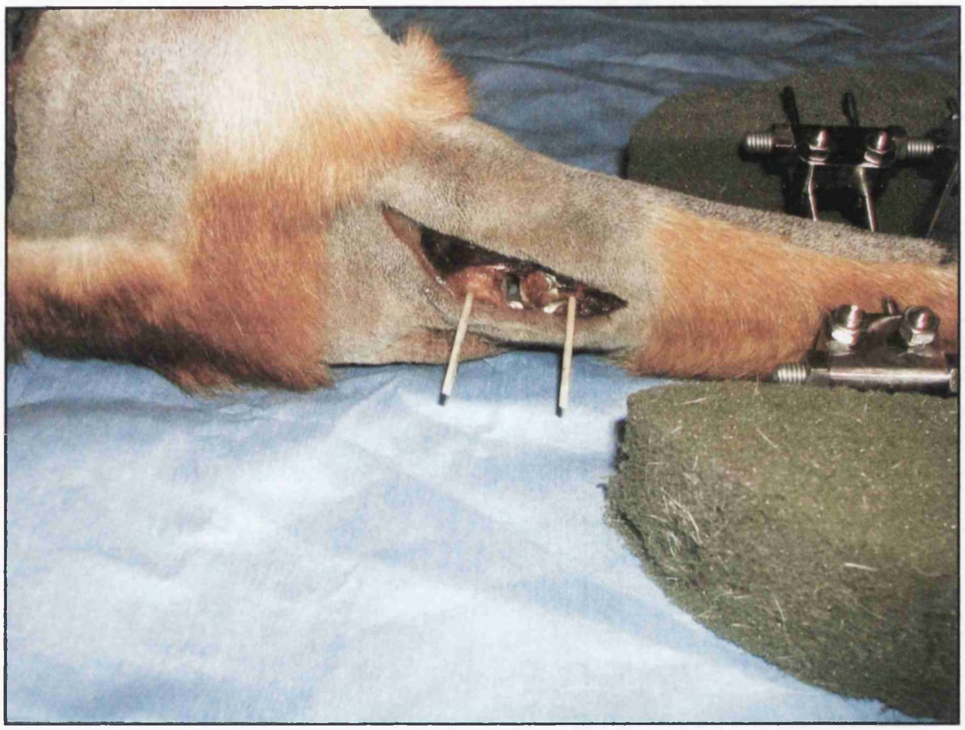

The elbows were positioned for scanning in slight extension in pairs using foam wedges (Figure 5). Scans were planned using a craniocaudal survey view, and covered the elbow joint from the anconeus proximally to a point distal to the proximal radioulnar articulation (Figure 1). The elbows were initially scanned with the linear motors locked off, *ie* with no induced incongruency. Following the initial scan, the linear motors on both elbows were used to reduce the radial ostectomy gap by 1 mm. This shortening was measured from the radial marker wires using Vernier callipers which were accurate to 0.1 mm (Figure 6). The presence of the medial coronoid process prevented distal movement of the humeral condyle. A corresponding increase in the humeroradial joint space was confirmed by measuring between the humeral and radial radiolucent markers. The CT scan was then repeated. This protocol was repeated for 1 mm increments up to a maximum of 4 mm of radial shortening. This allowed the collection of sequential CT scans of four elbows with induced radioulnar incongruencies of 0, 1, 2, 3 and 4 mm.

Figure 5 Forelimbs positioned for scanning in pairs

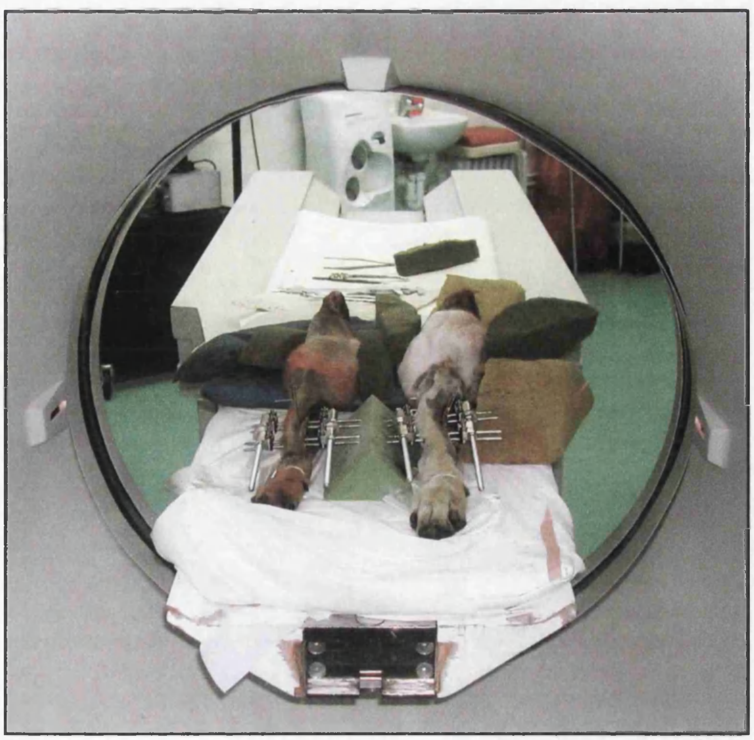

Figure 6 Vernier callipers used to measure radial shortening

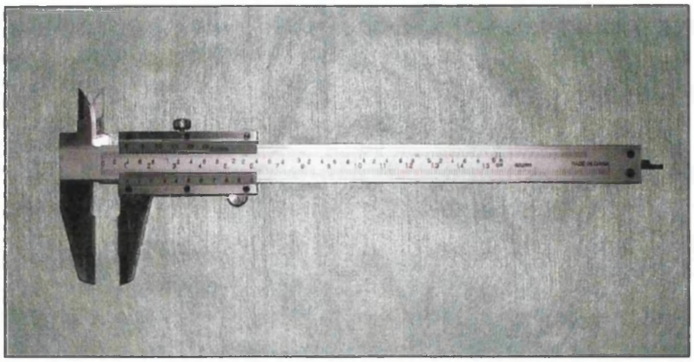

After the final scan was completed, the elbows were inspected to confirm the presence of a radioulnar incongruency (Figure 7)

Following collection, transverse CT scans were archived using standard software (OmniPro, CA, USA) until the time of analysis.

Figure 7 Gross radioulnar incongruency apparent after 4 mm of radial shortening. The white arrow indicates a radiocoronoid step

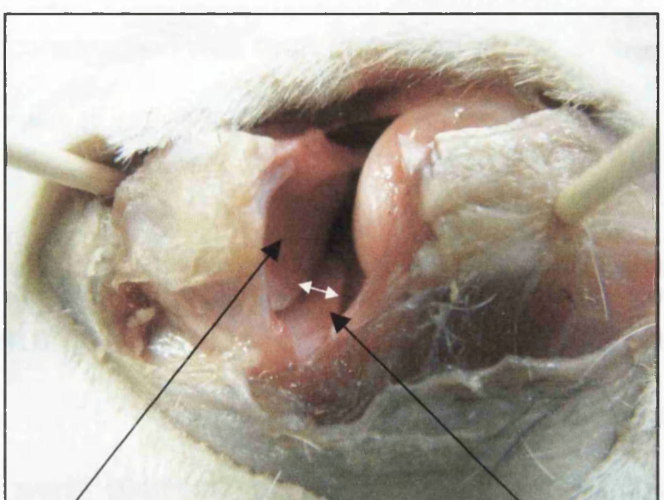

Radial Head

Medial coronoid process

(v) Post collection computed tomography reconstructions

Scans were retrieved from the archives and reviewed using image analysis software (OmniPro, CA, USA). For each elbow, the transverse CT slices were loaded into a multiplanar reconstruction program. Images were reviewed using a bone setting (window width 3500 Hounsfield units, window level 500 Hounsfield units).

Frontal and sagittal plane reconstructions were created in a standardized fashion. The transverse slice through the most cranial aspect of the medial coronoid process (the apex of the coronoid process) was identified. From this slice, the long axis of the coronoid process (LAC) was identified (Figure 8). The junction between the medial and lateral components of the coronoid process was then identified (Figure 9) and for phase 1 of the study, this point was taken to mark the level of the base of the coronoid process. A line was imposed through the base of the coronoid at 90^{o} to the LAC. The frontal plane reconstruction was then formatted at 90^{0} to the LAC, half way between the apex and the line through the base of the coronoid (Figures 10 and 11). A sagittal plane reconstruction was then formatted at 45^{0} to the LAC at the level of the coronoid base (Figures 12 and 13).

Using image analysis tools (OmniPro, CA, USA) the humeroradial (HR) and humeroulnar (HU) joint spaces on each reconstruction were measured (Figures 14 and 15). On frontal plane reconstructions, joint space measurements were obtained at the centre point of the HR and HU articulations respectively (giving FrHR and FrHU values). On sagittal plane reconstructions, joint space measurements were obtained 1 mm either side of the radioulnar articulation (giving SagHR and SagHU values).

Figure 8 Transverse CT slice through the apex of the medial coronoid process. The long axis of the coronoid process (LAC) is identified (red line)

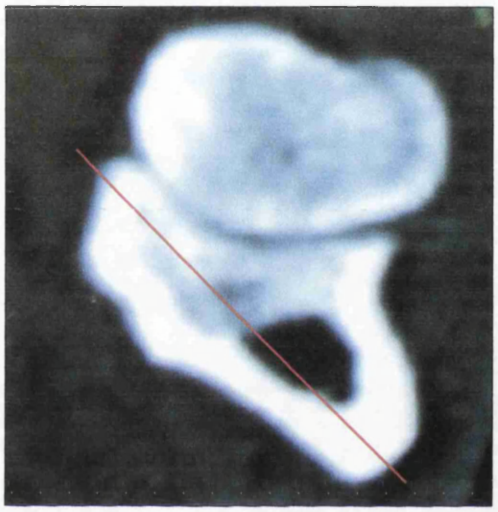

Figure 9 Transverse CT slice through the apex of the medial coronoid process. The junction between the medial and lateral components of the coronoid process is identified (black arrow)

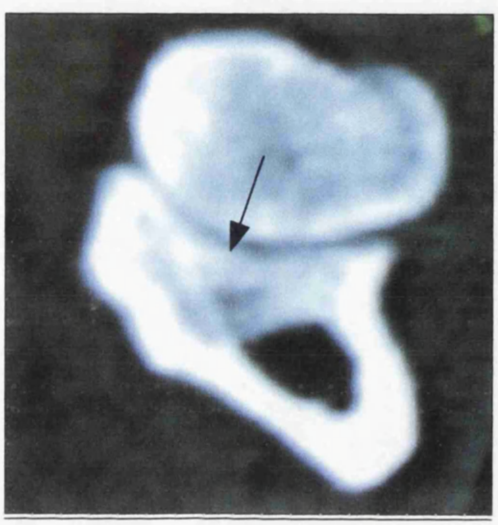

Figure 10 Transverse CT slice through the apex of the medial coronoid process. The level of the frontal plane reconstruction is identified at 90^0 to the LAC half way between the coronoid base and apex

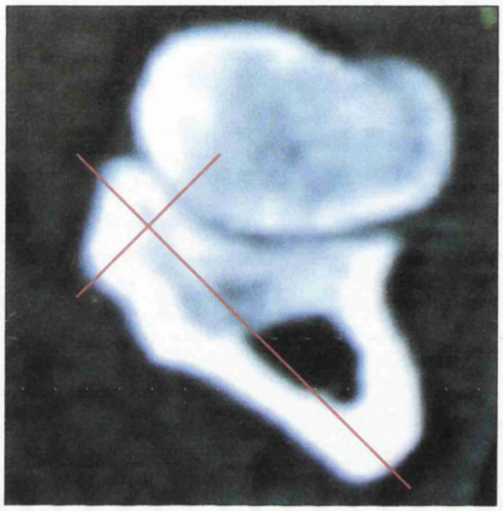

Figure 11 Frontal plane reconstruction

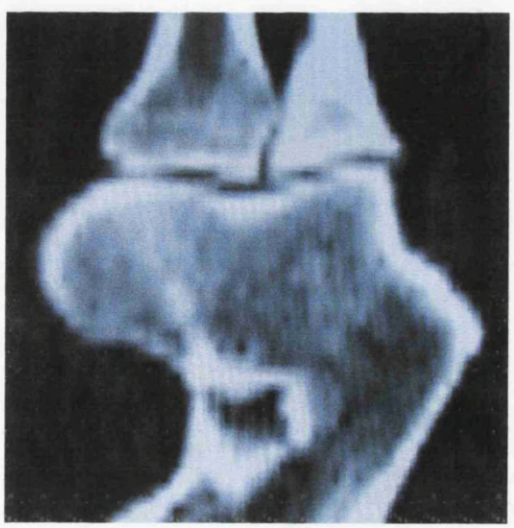

Figure 12 The sagittal plane reconstruction was formatted at 45^0 to the LAC at the level of the coronoid base

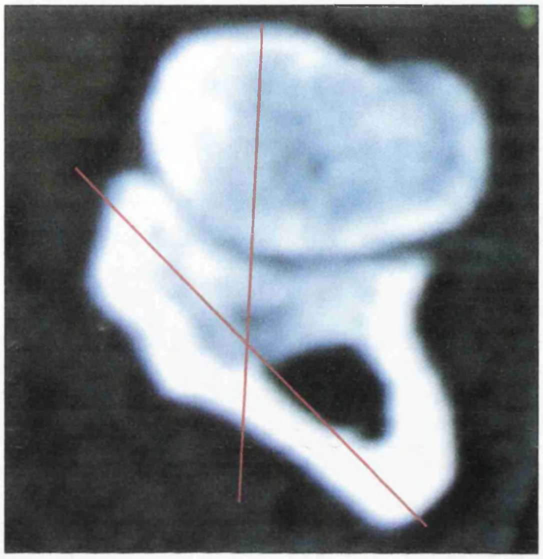

Figure 13 Sagittal plane reconstruction

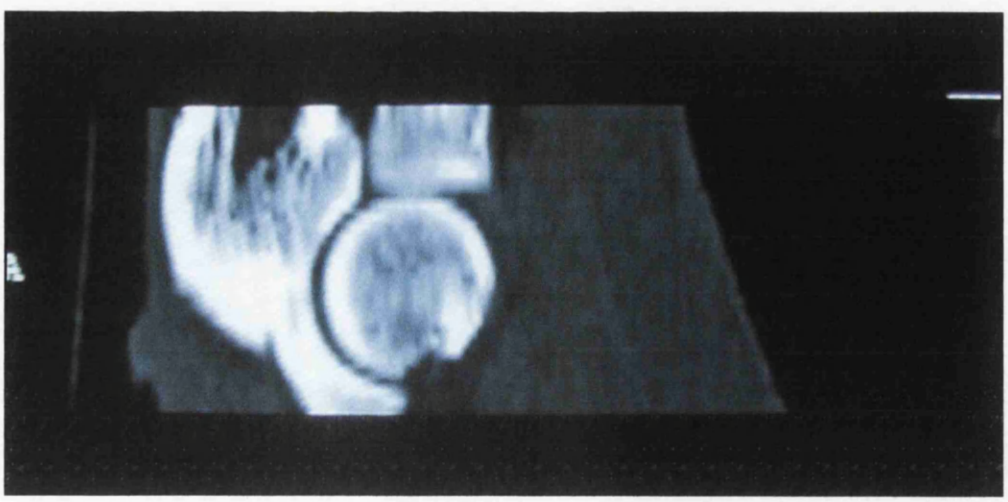

Figure 14 HR and HU joint space measurements obtained from frontal plane reconstructions at the centre of the HR and HU articulations respectively (red arrows)

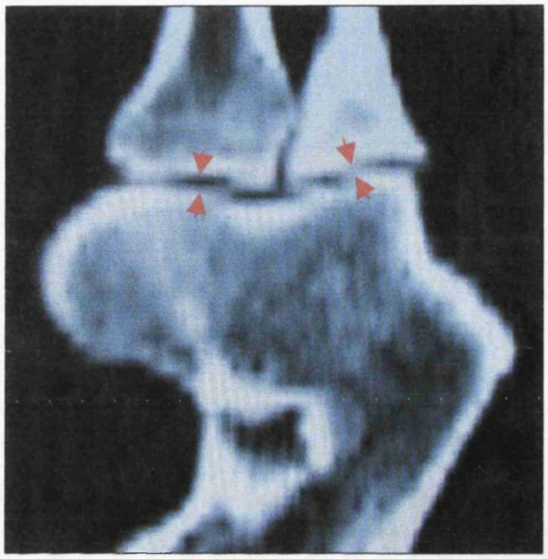

Figure 15 HR and HU joint space measurements obtained from sagittal plane reconstructions 1 mm either side of the radioulnar articulation (red arrows)

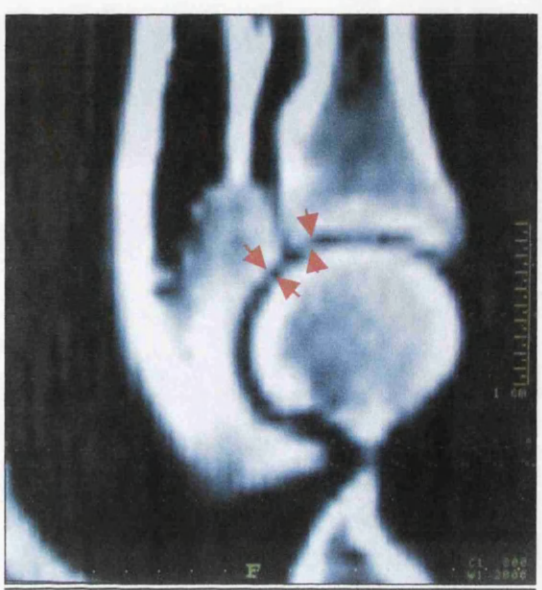

(vi) *Collection of frozen sections*

Following scanning, the eight elbows which had not been used for the induced incongruency section of the study were frozen in slight extension at -20^0 centigrade (elbows 2, 3, 4, 5, 6, 8, 11 and 12). The elbows were stored for 72 hours until the time of testing.

From the radiographic study (Materials and methods section (ii)), measurements were obtained for each elbow from the proximal aspect of the olecranon to a point four centimetres distal to the coronoid process and to a point four centimetres proximal to the supratrochlear foramen. Using a band saw, the antebrachium and the distal humerus were sectioned in the transverse plane at these points.

Using the visible cut ends of the radius and ulna and the palpable olecranon process as reference points, each elbow was then sectioned using the band saw. Four elbows were sectioned in the frontal plane through the mid-point of the medial coronoid process (elbows 3, 5, 11 and 12). The other four elbows were sectioned in the sagittal plane through the base of the coronoid process (elbows 2, 4, 6 and 8).

The frontal and sagittal plane cut surfaces of the elbows were cleaned with moistened swabs to remove ice crystals. Using Vernier callipers, the bone-to-bone HU and HR joint spaces were measured and recorded. Measurements were taken at the mid-point of the articulations on the frontal sections (Figure 16), and 1 mm either side of the radioulnar joint on the sagittal section (Figure

17). The specimens were then photographed using a 3-megapixel digital camera (Nikon Coolpix 885, Nikon Corporation, Japan).

Figure 16 HR and HU measurements obtained from frontal plane frozen sections (black arrows)

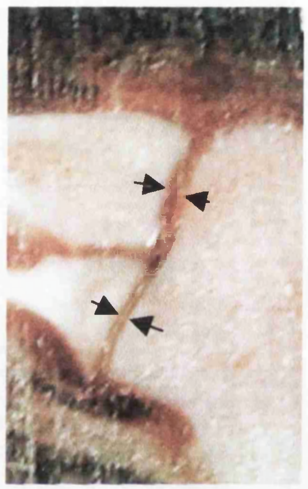

Figure 17 HR and HU measurements obtained from sagittal plane frozen sections (black arrows)

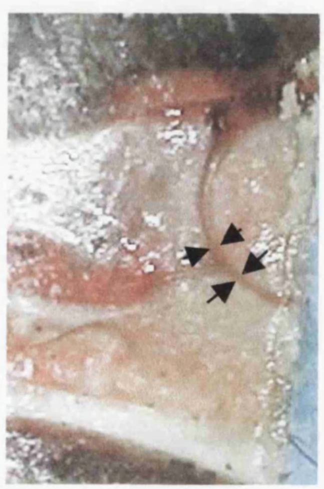

The elbows were then sectioned in the transverse plane through the centre of the humeral condyle. The transverse cross-sections were then photographed (Figure 18) and the images stored to assist with accurate orientation of rCT images.

Figure 18 Cross-section through the humeral condyle showing level of sectioning. These images assisted orientation of the rCT formatting

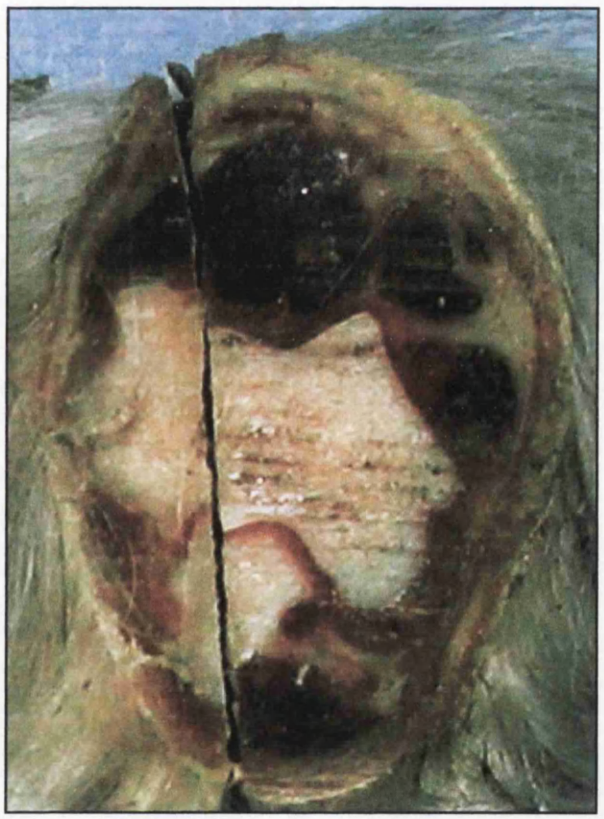

(vii) Inter-image variation analysis

Four elbows (elbows 2, 4, 5 and 8) were selected to assess the effect of positioning of the specimens and of image acquisition on the rCT images. Each elbow was scanned using the protocol described above (Materials and methods section (iii)). After scanning, the elbows were removed from the machine, repositioned, and the scan repeated. This was then repeated again to give a total of three scans for each elbow, or 12 scans in total.

Frontal and sagittal plane reconstructed images were formatted as described above (Materials and Methods section (v)) for each scan. From the rCT images, FrHR, FrHU, SagHR and SagHU joint spaces were measured and recorded.

The joint space measurements were then compared for each elbow on the three separate occasions. For each occasion, the data was recorded as 16 data points (Appendix 1). Correlation between the data was assessed graphically and using Pearson correlation coefficients. Variation between the data was further assessed graphically using a modified Bland and Altman plot: the variation between linked data points was calculated (defined as the difference between the maximum and minimum joint space values obtained for a given point). This variation was then plotted along a standardised x-axis (Figure 28). In addition, the standard deviation of variation was also calculated.

(viii) Inter-observer variation analysis

Four elbows (elbows 2, 4, 5 and 8) were selected to assess inter-observer variation. The first observer (TJG) reviewed a single scan for each elbow. rCT images were obtained as described above (Materials and Methods section (v)), and FrHR, FrHU, SagHR and SagHU joint space measurements recorded.

A second observer (GH) then reviewed the scans. rCT images were formatted, and joint space measurements obtained and recorded in a similar fashion.

The data for the two observers were recorded as 16 data points (Appendix 3). Correlation between the two observers was assessed graphically and using Pearson correlation coefficients. Variation between the data was further assessed graphically using a modified Bland and Altman plot: the variation (difference) between linked data points was calculated and this variation plotted along a standardised x-axis (Figure 30). In addition, the standard deviation of variation was also calculated.

(ix) Intra-observer variation analysis

Four elbows (elbows 2, 4, 5 and 8) were selected to assess the intra-observer variation. A single scan was reviewed for each elbow. rCT images were obtained as described above (Materials and Methods section (v)), and FrHR, FrHU, SagHR and SagHU joint space measurements recorded.

On a second occasion, the same observer (TJG) again reviewed the scans. rCT images were obtained, and joint space measurements recorded as described above.

The data from each occasion were recorded as 16 data points (Appendix 4). Correlation between the data was assessed graphically and using Pearson correlation coefficients. Variation between the data was further assessed graphically using a modified Bland and Altman plot: the variation (difference) between linked data points was calculated, and this variation plotted along a standardised x-axis (Figure 32). In addition, the standard deviation of variation was also calculated.

(x) Comparison of reconstructed images with frozen sections

As described above (Materials and Methods section (vi)), eight elbows were selected. Four elbows were then randomly selected for comparison of frontal plane images (elbows 3, 5, 11 and 12) and four for comparison of sagittal plane images (elbows 2, 4, 6 and 8). Using the digital images of the transverse frozen sections through the humeral condyle and the radius and ulna as guides, rCT images were formatted in the frontal plane (elbows 3, 5, 11 and 12) and in the sagittal plane (elbows 2, 4, 6 and 8) at the same levels as the frozen sections.

Digital photographs of the distal elbow articulation were recorded from the rCT images. These photographs were then visually compared with the corresponding frozen section photographs which had been recorded previously (Materials and methods section (vi)).

FrHR, FrHU, SagHR and SagHU joint space measurements were obtained from the rCT images as described above (Materials and methods section v). These measurements were compared with the corresponding joint space measurements obtained from the frozen sections (Materials and Methods section vi). The data were recorded as 16 data points (Appendix 6). Correlations between the data from the rCT images and the frozen sections were then compared graphically and using Pearson correlation coefficients. Variation between the data was further assessed graphically using a modified Bland and Altman plot: the variation (difference) between linked data points was calculated, and this variation plotted along a standardised x-axis (Figure 35). In addition, the standard deviation of variation was also calculated.

(xi) <u>*Analysis of detection of incongruencies*</u>

Using four elbows (elbows 1, 7, 9 and 10) scans of the elbows were obtained for each incremental degree of radial shortening as described above (Materials and Methods section (iv)). For each scan, rCT images were formatted and FrHR and SagHR joint space measurements obtained from the images.

On the frontal plane reconstructions, FrHU joint space measurements were also recorded. A calculation of joint incongruency (JI) was then made by subtracting the FrHU joint space measurement from the FrHR joint space measurement (giving a JIFr value). Because small craniocaudal movements of the humerus during radial shortening were not accurately controlled (Figure 19), HU joint space measurements from sagittal plane reconstructions (SagHU) were not constant and therefore changes in JI on sagittal reconstructions could not be directly assessed using this model.

A direct measurement of radioulnar incongruency (JIRU) was also made from the sagittal reconstructions. This measurement was made from the border of the coronoid process to the radial head (Figure 19).

<u>Figure 19</u> Sagittal plane rCT (elbow 9 after 3 mm of radial shortening) showing direct measurement of radioulnar joint space (red arrow). Slight cranial movement of the humeral condyle away from the trochlear groove can be clearly seen (white arrow).

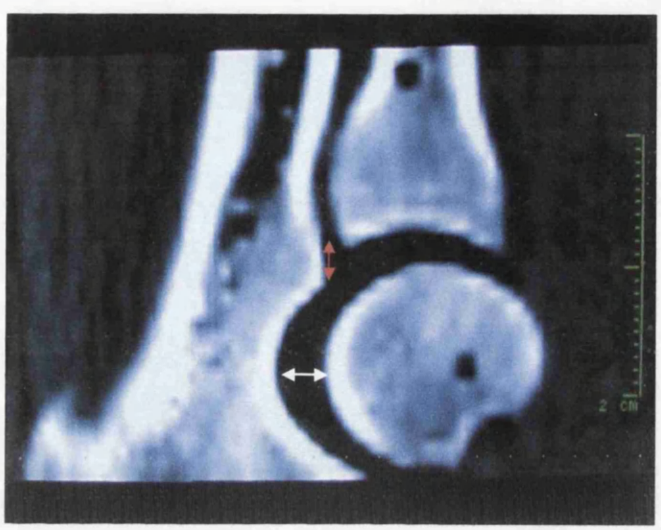

The values for FrHR, SagHR, JIFr and JIRU for each elbow were recorded. From these figures, the increase in FrHR, SagHR, JIFr and JIRU from the baseline figures was recorded for each incremental degree of radial shortening (giving iFrHR, iSagHR, iJIFr and iJIRU values). These values were compared with the known values of radial shortening, and hence the known induced incongruency. The correlation between the induced incongruency and iFrHR, iSagHR, iJIFr and iJIRU was assessed graphically. In addition, variation between iFrHR, iSagHR, iJIFr and iJIRU and the known increase in induced incongruency was further assessed graphically using Bland and Altman plots.

Phase Two - Retrospective Clinical Study

(i) Identification of Affected and Control elbows

The clinical database at the University of Glasgow Veterinary School (GUVS) was reviewed over a three year period (2000-2003) to identify dogs which had had CT and radiographic evaluation of the elbow joint. Additional clinical information collected included age, breed, sex and weight of dogs and the clinical diagnoses.

Radiographic evaluation included flexed and neutral mediolateral and extended craniocaudal views of the elbows. Radiographs were obtained with the dogs under heavy sedation or general anaesthesia. Dogs were positioned using sandbags and foam wedges; manual restraint was not employed. CT scans were obtained using the Exel 2400 elite scanner (Elscint Ltd, Haifa, Israel). Dogs were anaesthetised and placed in either ventral or lateral recumbency. One or both elbows were scanned with the elbows perpendicular to the CT gantry in moderate extension. The head was pulled caudally to avoid interference with the scan (de Rycke and others 2002). Scans were planned from a craniocaudal survey view and included a minimum of 12 CT slices centred over the distal elbow joint (Figure 20). Slice thickness was 1.2 mm; bed increment was 1.0 mm. To minimise variation, the scans were reviewed by a single observer (TJG) using a bone setting (window width 3500 Hounsfield units, window level 500 Hounsfield units).

Figure 20 Craniocaudal survey view demonstrating region to be scanned in the clinical patients

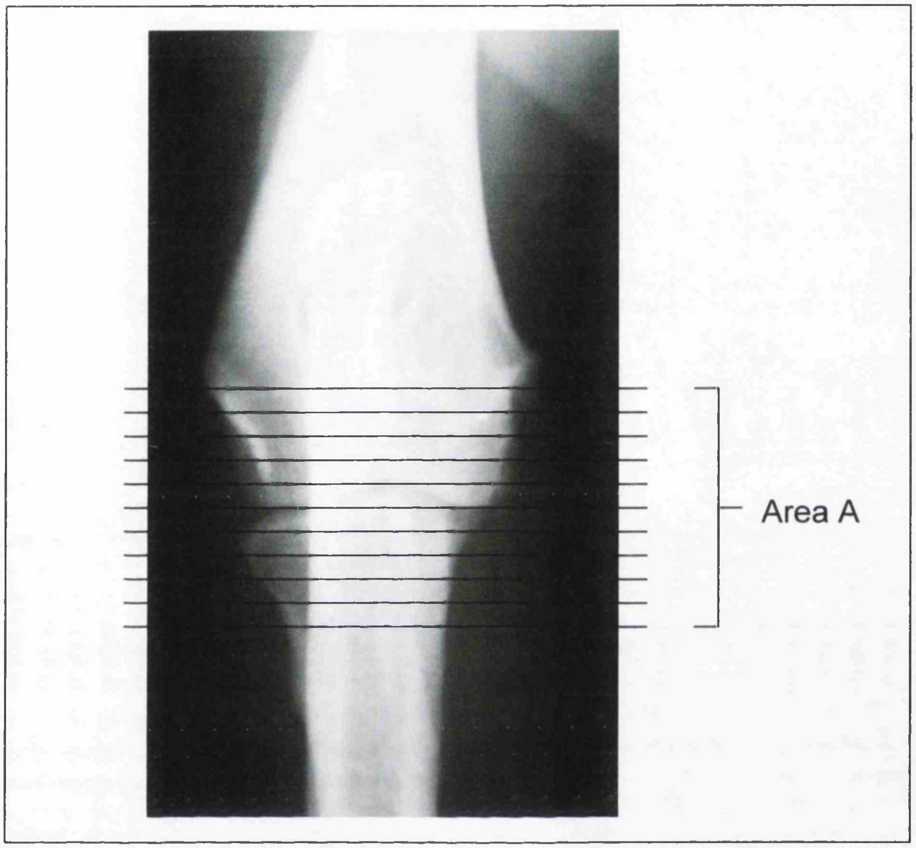

Based on evaluation of the radiographs and transverse CT scans (Olsson 1983, Henry 1984, Korbel and others 2001, Rovesti and others 2002, de Rycke and others 2002) and of clinical information, elbows were assigned to either a coronoid disease (CD) group or a control group (Figure 21). Elbows diagnosed with other conditions such as trauma, UAP, OCD or incomplete ossification of the humeral condyle (IOHC) were excluded from the study. Elbows in which a diagnosis was uncertain (*eg* where radiographic changes were absent but clinical information indicated elbow pain) were also excluded.

Figure 21 Table detailing criteria for assignment of elbows to control or CD groups

	Control elbows	*CD elbows*
Clinical examination		
Lameness	-	+
Pain on manipulation	-	+
Joint effusion	-	+/-
Radiographic examination		
Osteophyte formation on anconeus (flexed mediolateral view)	-	+
Subcoronoid or subtrochlear sclerosis	-	+
Osteophyte formation on medial epicondylar ridge (CrCd view)	-	+
Identification of coronoid fragmentation	-	+/-
CT examination		
Identification of coronoid fragmentation	-	+/-
Osteophyte formation on proximal radius or ulna, or distal humerus	-	+
Irregular shape of the coronoid process	-	+

(ii) Collection of Reconstructed Computed Tomography Images

To allow evaluation of different areas of the elbow joint, a more detailed method of formatting standardised reconstructions was devised. The CT slice through the apex of the coronoid process was identified and the LAC identified. Standardised reconstructions were then formatted at 90 degrees to this axis in the frontal plane at the level of the coronoid apex (FrA) and further caudally at the coronoid base (FrB) (Figure 22). The FrA images were reconstructed 1.0 mm caudal to the coronoid apex. In the event of identification of a coronoid fragment on the transverse CT slice, the FrA image was reconstructed 0.5 mm below the fissure line. For this clinical phase of the study, the level of the FrB image was determined by analysing more proximal transverse CT scans through the centre of the trochlear notch. The most caudal point of the centre of the humeral condyle was then identified (Figure 23) and the FrB image reconstructed level with this point. A third reconstruction was formatted at 45 degrees to the coronoid long axis in the sagittal plane at the coronoid base (SagB). This reconstruction was 1 mm medial to the junction of the medial and central components of the coronoid process (Figure 24).

Figure 22 Transverse CT slice through the apex of the medial coronoid process. The levels of the apical and basal frontal reconstructions (FrA and FrB) are identified

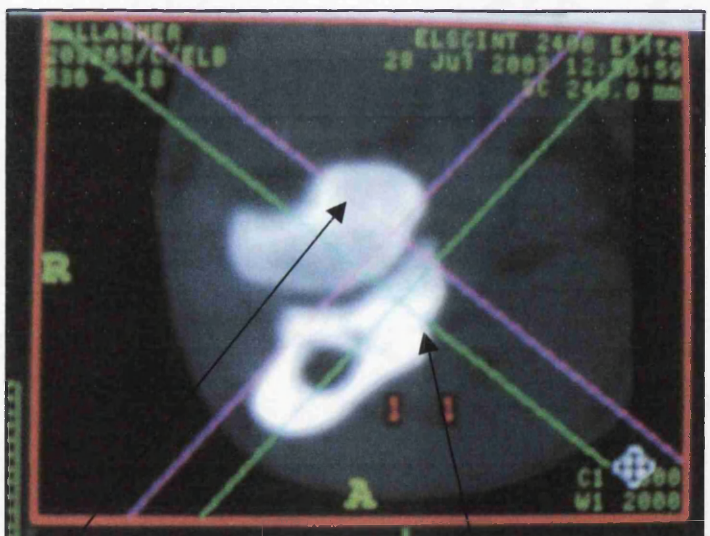

Level of FrA reconstruction

Level of FrB reconstruction

Figure 23 Transverse CT slice through the centre of the trochlear notch. The FrB image was formatted level with the most caudal point of the centre of the humeral condyle at 90 degrees to the LAC (line A)

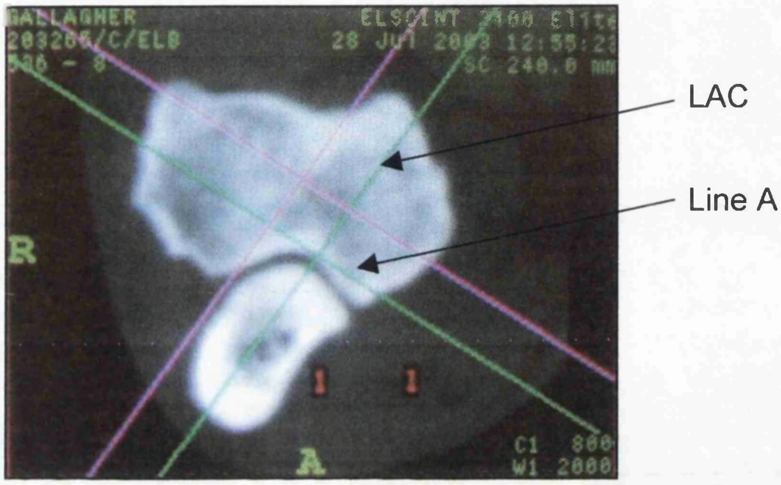

Figure 24 Transverse CT slice through the apex of the medial coronoid process. The level of the sagittal plane reconstruction is identified (line S), 1 mm medial to the junction of the medial and lateral components of the coronoid process

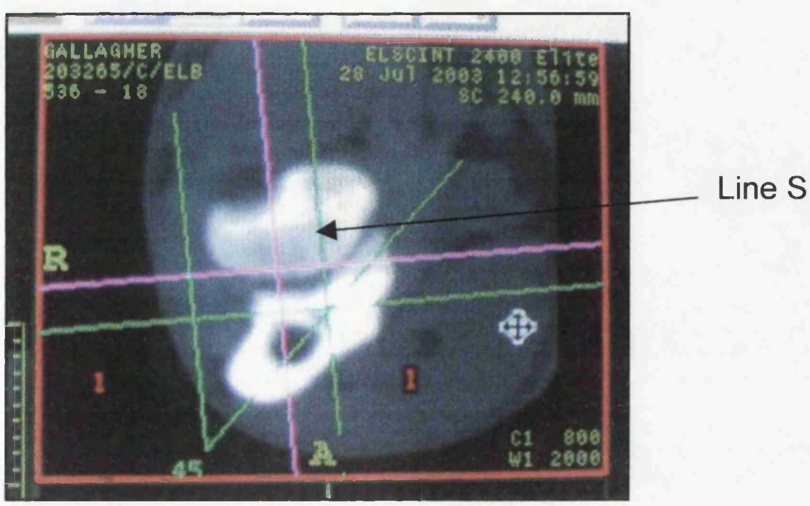

Using image analysis software (OmniPro, CA, USA) the HR and HU joint spaces on each reconstruction were measured (Figures 25 and 26). For each reconstruction, the difference between the HR joint space and the HU joint space was calculated to give a figure representing JI. The JI values for CD and control elbows were then compared and contrasted.

Figure 25 HR and HU joint space measurements obtained from the centre of the HR and HU articulations on frontal plane reconstructions (black arrows)

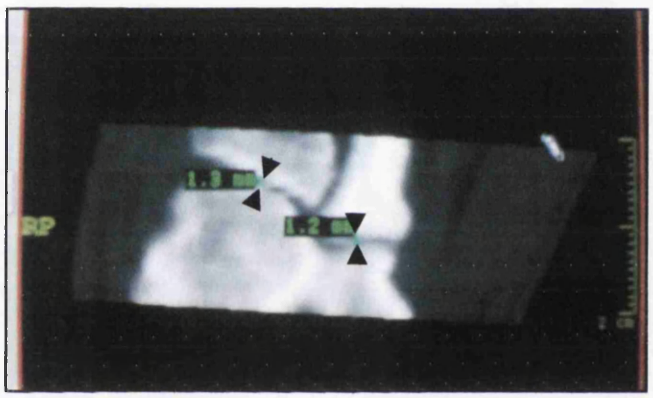

Figure 26 HR and HU joint space measurements obtained 1 mm either side of the radioulnar articulation on sagittal plane reconstructions (black arrows)

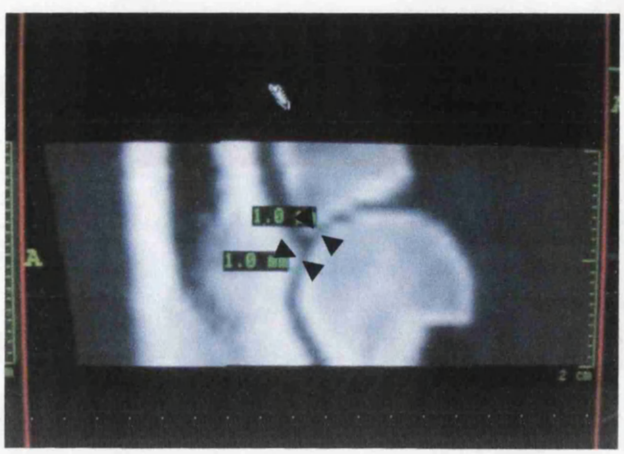

(iii) Statistical analysis

Distributions of age, weight, HR, HU and JI values were tested for normality both graphically and using the Anderson-Darling measure. There was sufficient evidence of non-normality to adopt a non-parametric approach to analysis.

CD and control data were compared for differences with respect to age and weight. In addition, the control data were analysed for association between age or weight and JI.

For each level of reconstruction (FrA, FrB and SagB), CD and control JI values were compared using a Mann-Whitney U test. For levels where significant differences were noted, absolute HR and HU values were then compared between CD and control groups, again using a Mann-Whitney U test.

In addition, JI values for different joint levels within CD and control groups were compared using the Kruskal Wallis test.

Results

Part One – Cadaver Study

(i) Population data, radiography and transverse CT scans

The 12 elbows were harvested from 6 cadavers. Clinical examination of the limbs was unremarkable, and all elbows had a normal range of motion. All cadavers were collie or collie-cross type dogs. The size of the cadavers ranged from medium to large, with bodyweights ranging from approximately 15 to 40 kg. No toy, small or giant dogs were included.

All radiographs were of excellent diagnostic quality. Evaluation of the radiographs excluded the presence of degenerative joint disease, as judged by an absence of osteophyte formation and subtrochlear sclerosis, in all elbows. Particular attention was paid to the anconeal process on the flexed mediolateral views and to the medial epicondylar ridge on the craniocaudal views when assessing osteophyte formation. None of the elbows exhibited radiographic evidence of joint incongruency. Evaluation of the transverse CT scans was unremarkable.

(ii) Inter-image variation analysis

The absolute joint space measurements are detailed in Appendix 1. Graphically, the measurements from different rCTs of the same elbows appear to correlate well (Figure 27). This correlation is supported statistically with R-values ranging from 0.70 to 0.80 for Pearson tests between the different sets of data (Appendix 2). The modified Bland and Altman plot indicates minimal variability between the different data sets (Figure 28). The standard deviation of the variation between linked data points was +/- 0.087 mm.

Figure 27 Graph showing joint space values from different rCTs of the same elbow

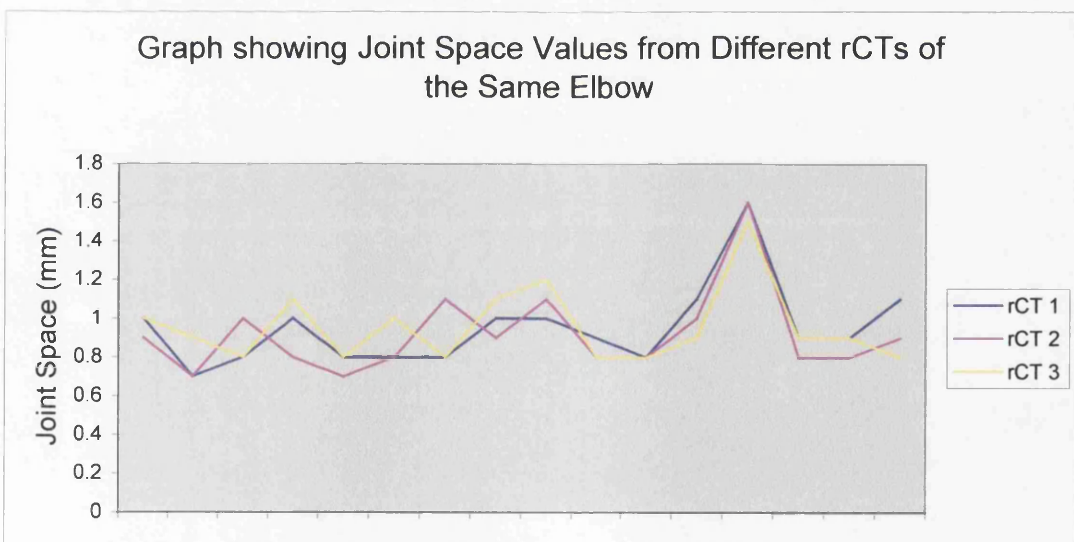

Figure 28 Modified Bland and Altman plot showing variation between different rCTs of the same elbow

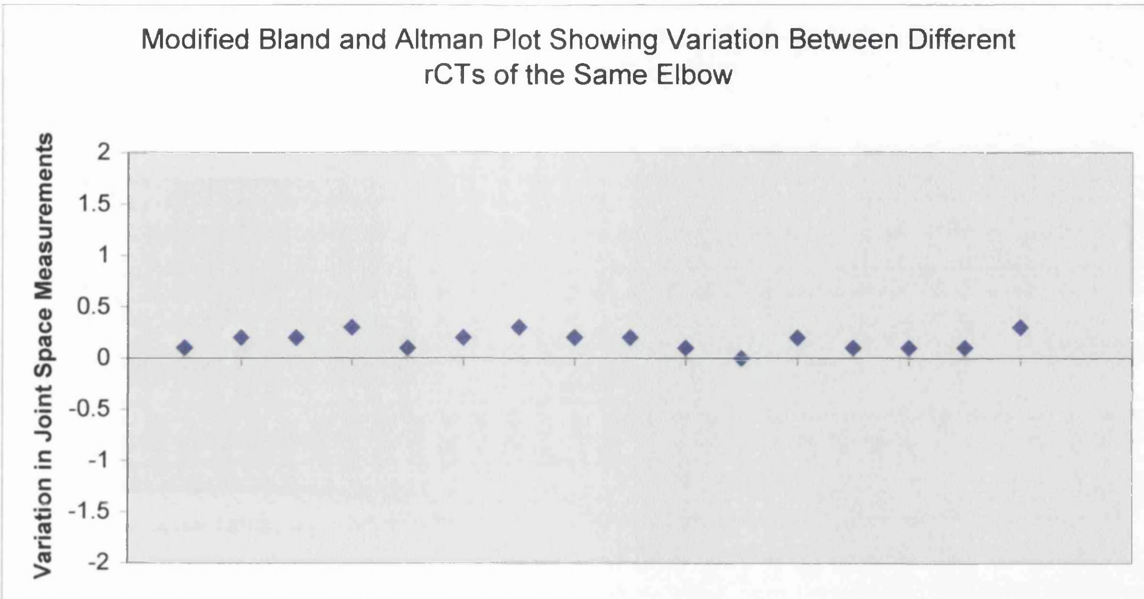

(iii) Inter-observer variation analysis

The absolute joint space measurements are detailed in Appendix 3. Graphically, the measurements from the two observers appear to agree reasonably well (Figure 29). The Pearson correlation coefficient for the two sets of data was R = 0.471, implying moderate agreement. The Bland and Altman plot indicates moderate variability between the different data sets (Figure 30). The standard deviation of the difference between paired data points was +/- 0.21 mm.

Figure 29 Graph showing measurements of the same elbows by different observers

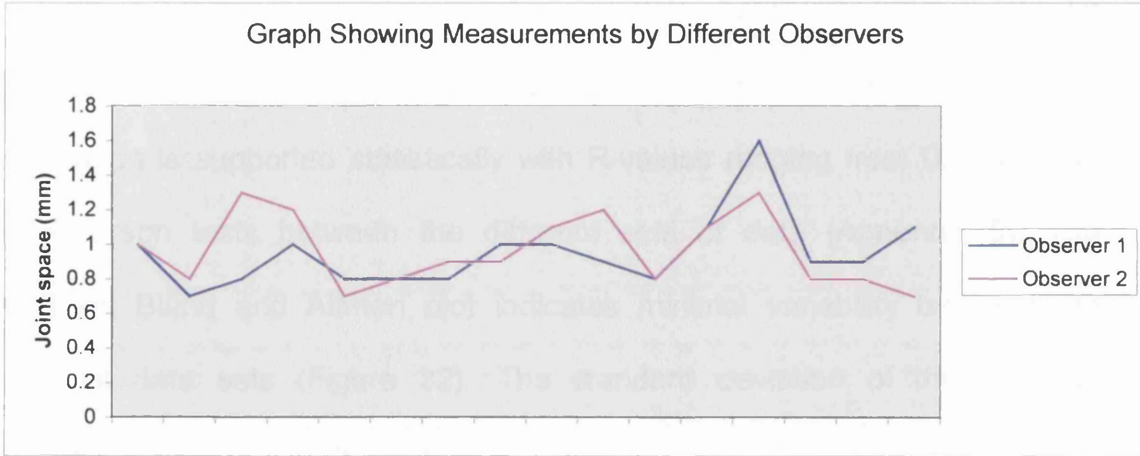

Figure 30 Modified Bland and Altman plot showing variation between different observers

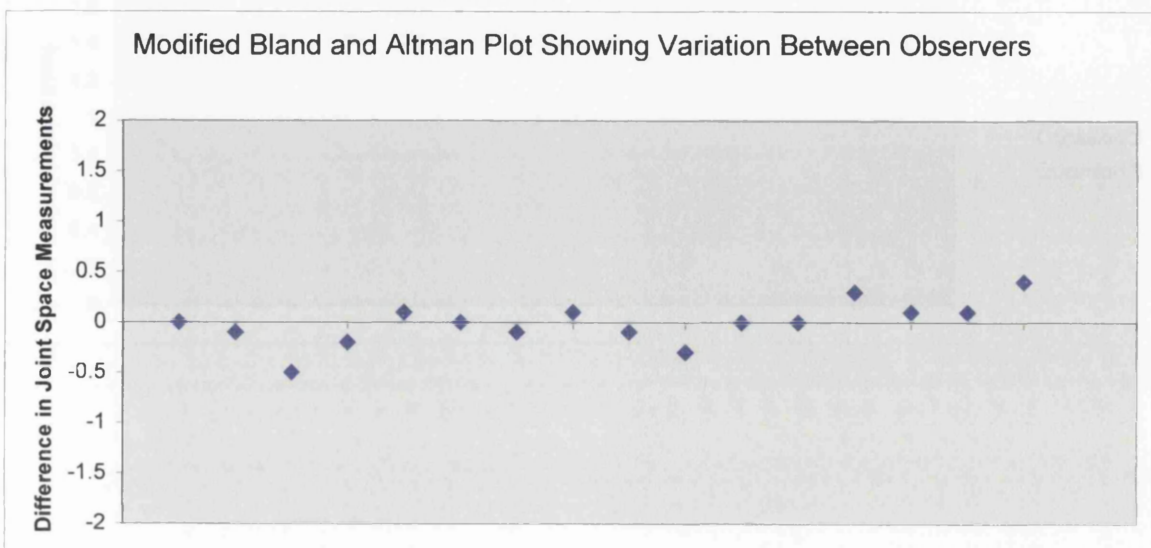

(iv) Intra-observer variation analysis

The absolute joint space measurements are detailed in Appendix 4. Graphically, the measurements obtained of the same elbows on different occasions by the same observer appear to correlate well (Figure 31). This correlation is supported statistically with R-values ranging from 0.77 to 0.92 for Pearson tests between the different sets of data (Appendix 5). The modified Bland and Altman plot indicates minimal variability between the different data sets (Figure 32). The standard deviation of the variation between linked data points was +/- 0.10 mm.

Figure 31 Graph showing joint space measurements by the same observer on three different occasions

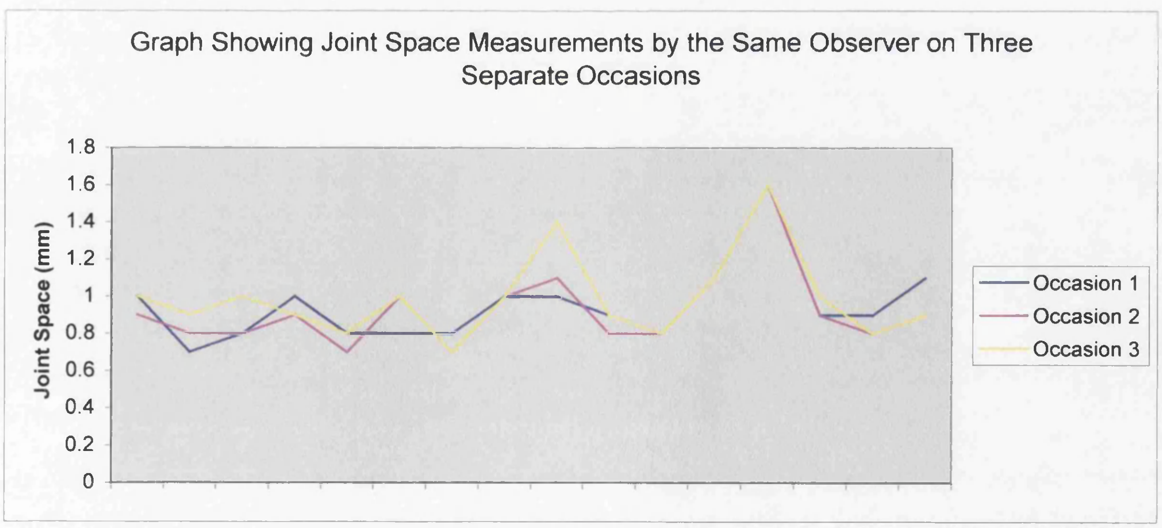

Figure 32 Modified Bland and Altman plots showing variation between joint space measurements by the same observer on three different occasions

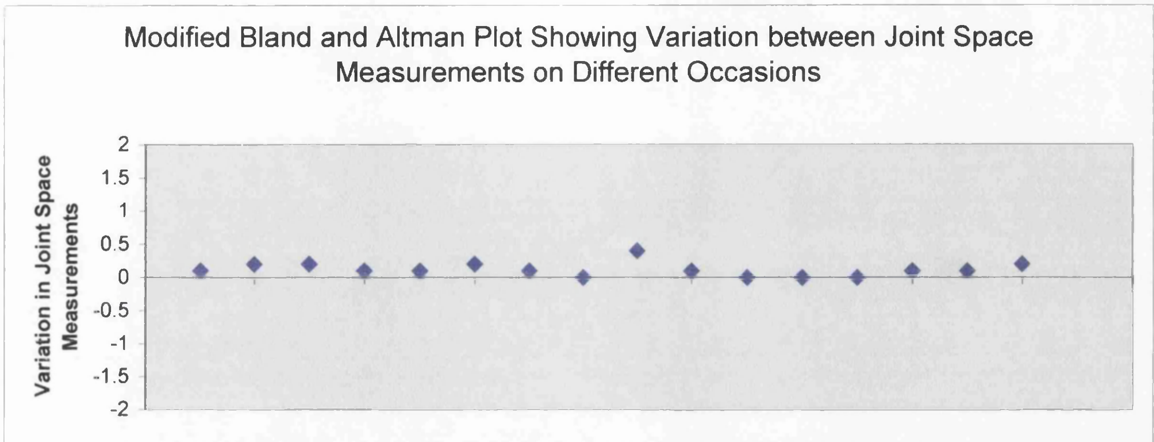

(v) Comparison of reconstructed images with frozen sections

Visually, the images obtained by rCT appeared to accurately reflect the corresponding frozen sections (Figure 33). The absolute joint space measurements are detailed in Appendix 6. Graphically, the measurements from the rCTs and frozen sections appear to correlate reasonably well (Figure 34). The Pearson correlation coefficient for the two sets of data was R = 0.88, implying good correlation. The modified Bland and Altman plot indicates minimal variability between the different data sets (Figure 35). The standard deviation of the difference between paired data points was +/- 0.14 mm.

<u>Figure 33</u> rCT images compared with corresponding frozen section images

<u>(i) Sagittal plane images</u>

Elbow 2

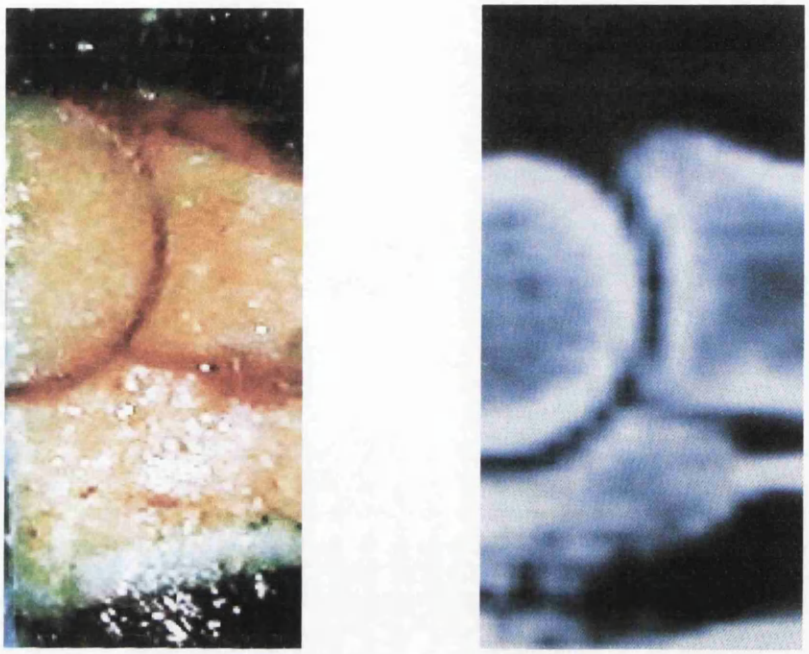

Elbow 4

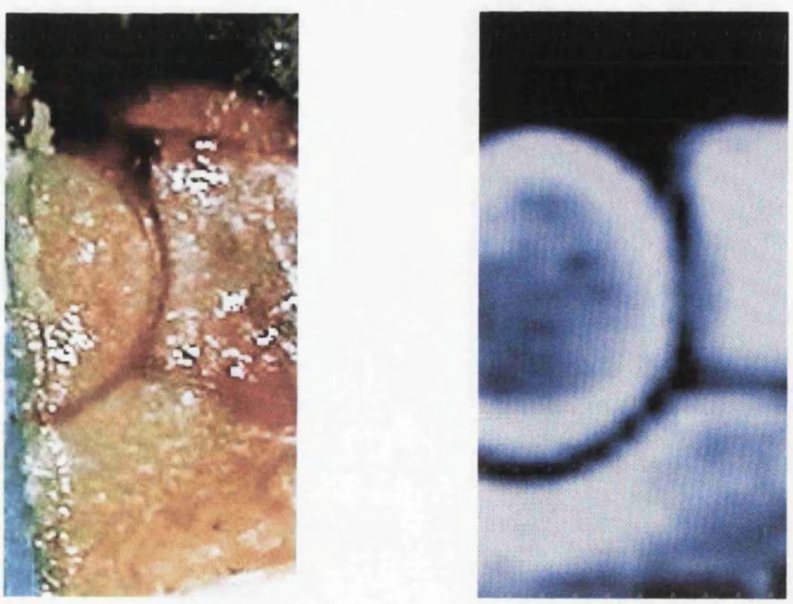

Elbow 6

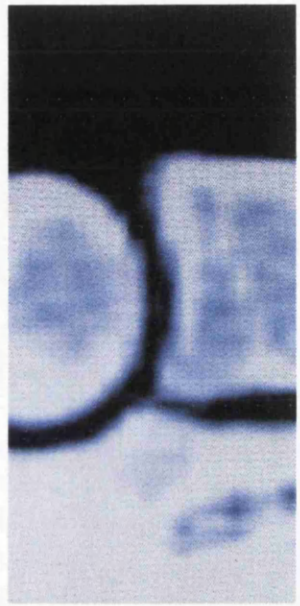

Elbow 8

Frontal plane images

Elbow 3

Elbow 5

Elbow 11

Elbow 12

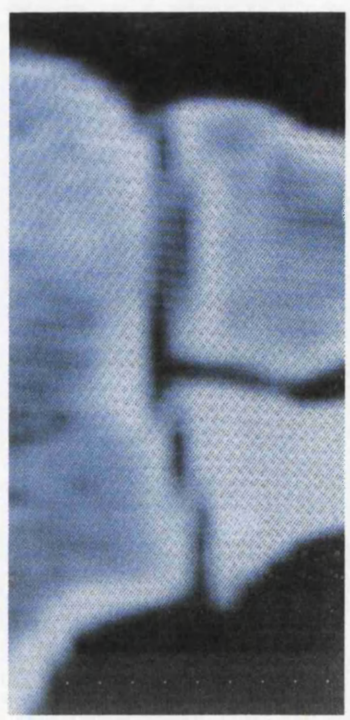

Figure 34 Graph showing joint space measurements from rCT and frozen sections

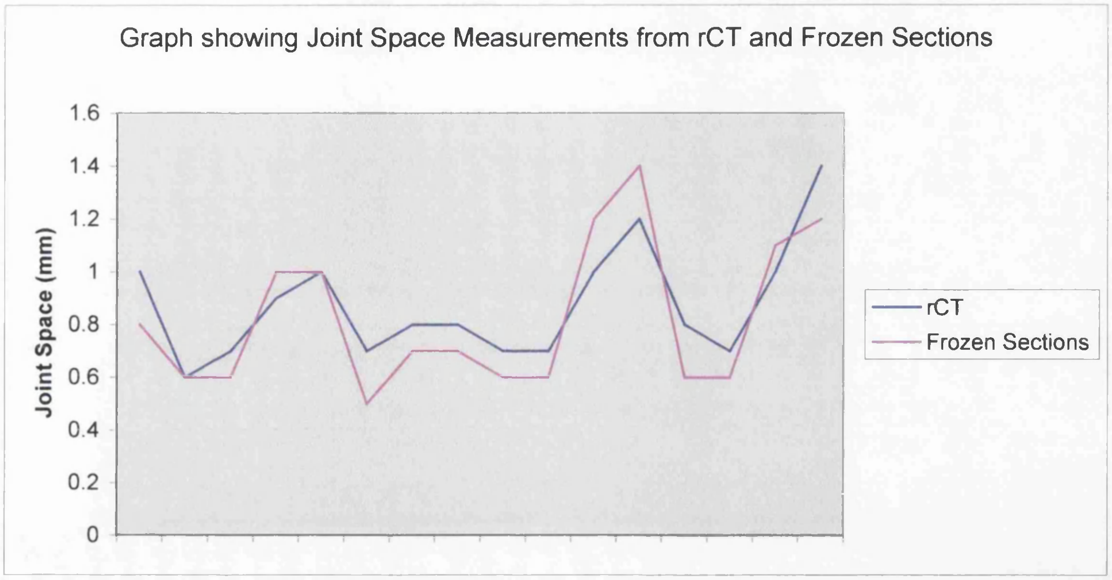

Figure 35 Modified Bland and Altman plot showing variation between rCT and frozen section measurements

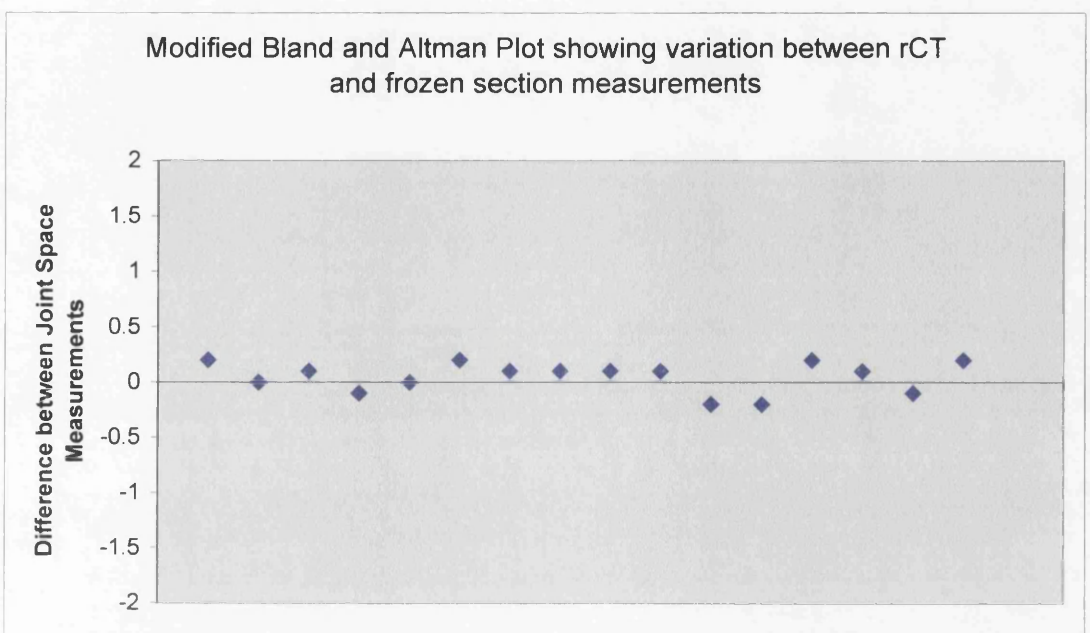

(vi) Analysis of detection of induced incongruencies

The FrHR and SagHR joint space measurements, the JIFr calculations and the JIRU measurements are detailed in Appendix 7. From these figures, the increase in FrHR, SagHR, JIFr and JIRU values from the baseline were calculated for each degree of radial shortening (Appendix 8). These figures (iFrHR, iSagHR, iJIFr and iJIRU) were then compared with the known radial shortening, and hence known incongruencies. Graphically, the iFrHR, iSagHR and iJIFr values appeared to correlate reasonably well with the induced incongruencies (Figure 36) although in all cases values were slightly decreased compared to the known incongruency. iJIRU exhibited poor agreement with the induced incongruencies. The Bland and Altman plots indicate iFrHR, iSagHR and iJIFr agreed closely with the induced incongruencies (Figures 37-39) though poor agreement was seen between iJIRU and induced incongruency (Figure 40).

Figure 36 Graph showing induced incongruencies versus measured joint spaces

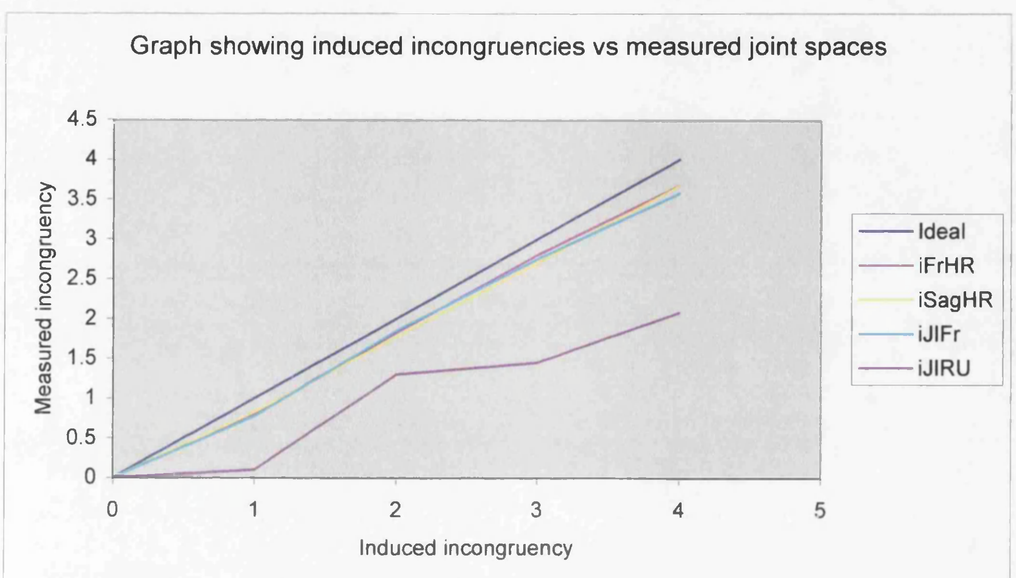

Figure 37 Bland and Altman plot of variation between FrHR and induced incongruency

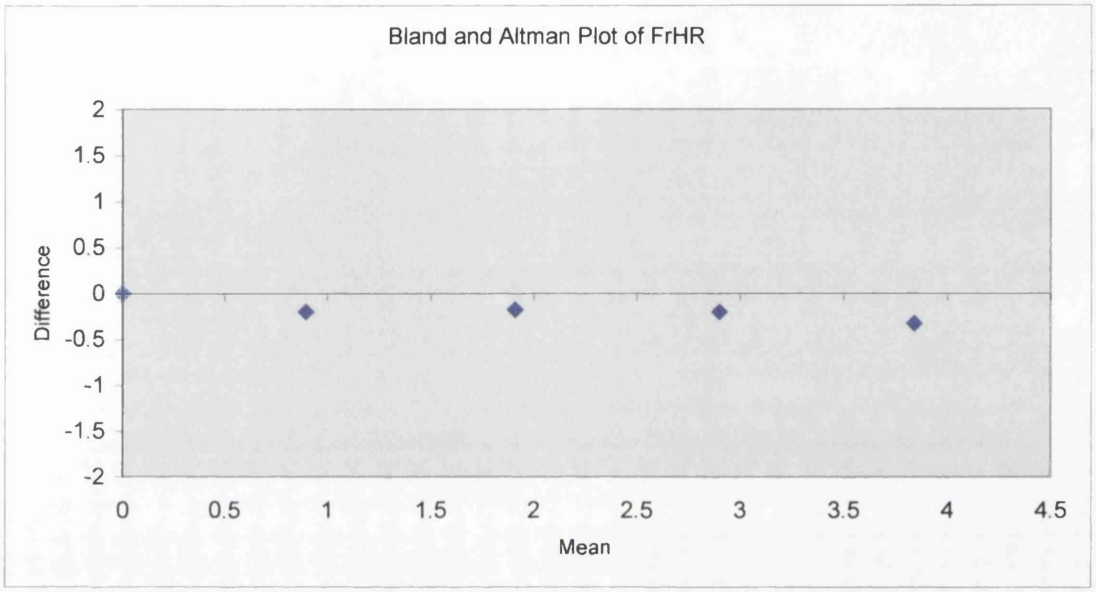

Figure 38 Bland and Altman plot of variation between SagHR and induced incongruency

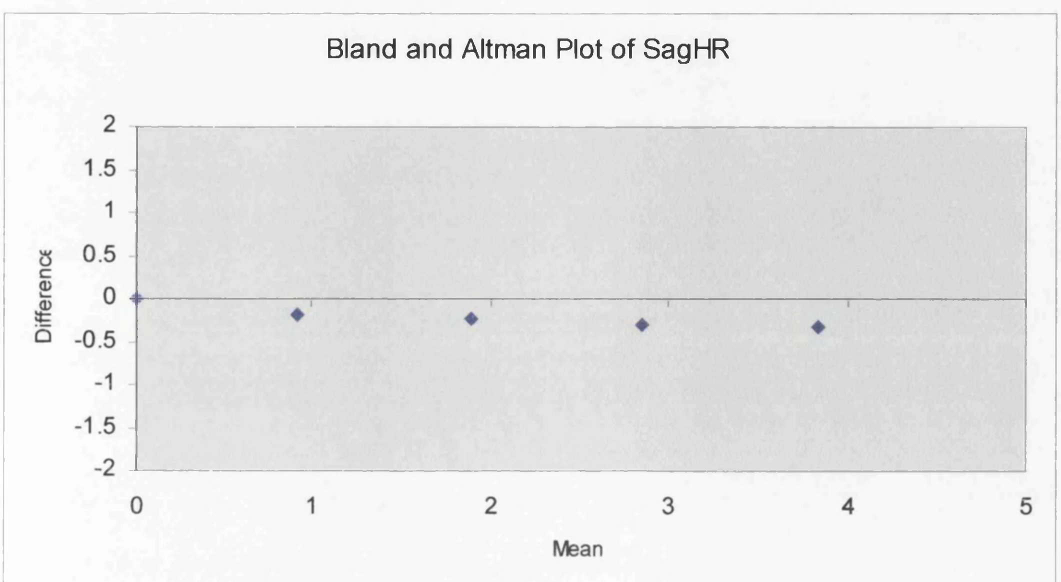

Figure 39 Bland and Altman plot of variation between iJIFr and induced incongruency

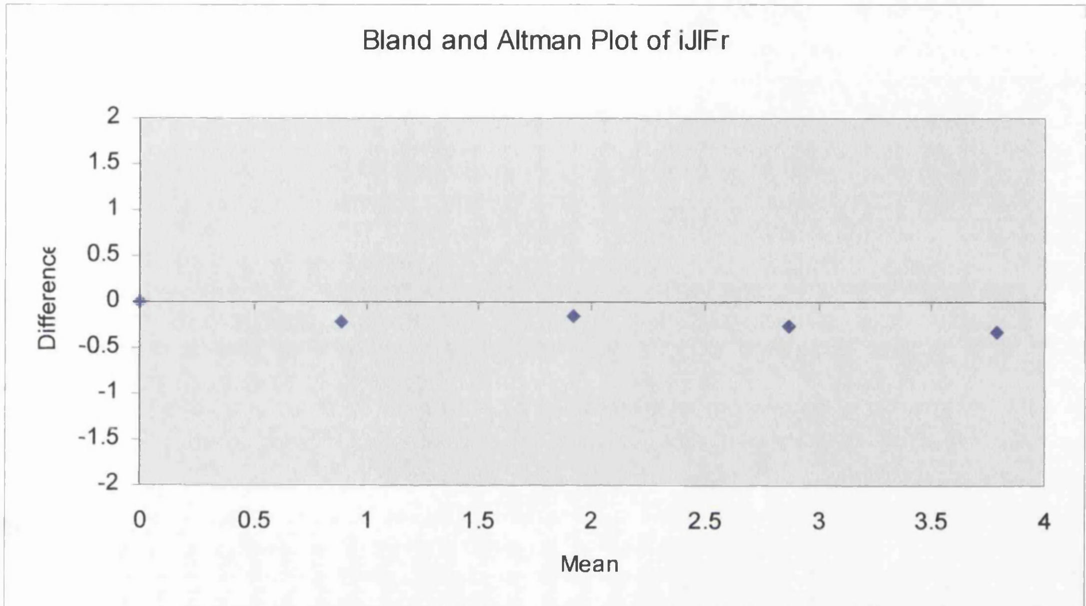

Figure 40 Bland and Altman plot of variation between iJIRU and induced incongruency

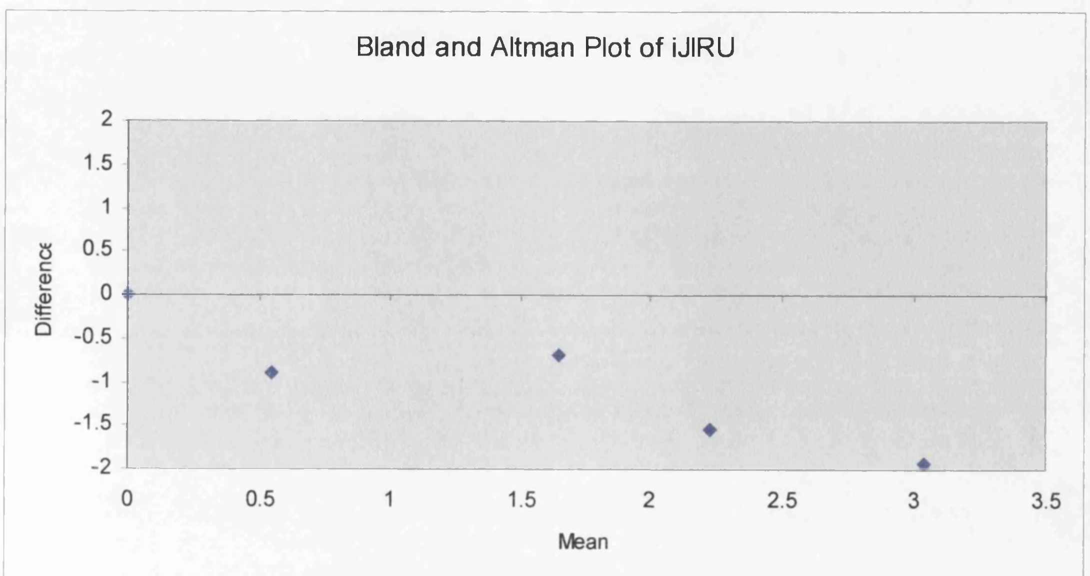

Part 2 - Retrospective Clinical Study

42 CD and 29 control elbows were identified. Median age was 12 months (range 6-49 months), and median weight 30 kg (range 11-55 kg). The JI values for CD and control dogs are detailed in Appendix 9. No significant difference was found between CD and control groups with respect to age, though CD dogs were slightly heavier than controls (median 31 kg vs 28 kg, $p=0.0005$). A variety of different breeds were identified (Figure 41). No relationship was noted between age or weight and JI values in the control elbows.

Figure 41 Breeds identified (frequency in brackets) for diseased and control elbows in the retrospective study

CD elbows	Control elbows
Labrador retriever (16)	Labrador Retriever (8)
Golden Retriever (9)	Golden Retriever (5)
German Shepherd Dog (4)	Springer Spaniel (5)
Mastiff (2)	Boxer (3)
Rottweiler (2)	Cavalier King Charles Spaniel (3)
Boxer (2)	German Shepherd Dog (2)
Clumber spaniel (2)	Rottweiler (1)
Crossbred (2)	Dalmation (1)
St Bernard (1)	Border Collie (1)
Bernese Mountain dog (1)	
Border Collie (1)	

When JI values for CD and control elbows were compared (Figure 42), no significant difference in incongruency was noted at the level of the coronoid base on frontal or sagittal reconstructions. At the level of the coronoid apex, CD elbows exhibited a radioulnar incongruency compared to controls (median 0.6 mm vs 0.0 mm, p<0.0001). However, incongruency was not present in all CD cases (Figure 43). JI at the coronoid apex in CD elbows was shown to be significantly greater (p<0.0001) than at the coronoid base (Figure 44) though no difference in JI was seen between different joint levels in control elbows. At the level of the coronoid apex, the HR joint space in CD elbows was significantly wider than controls (p=0.0006), although no difference was noted in the HU space (Figure 45).

<u>Figure 42</u> Median joint incongruency measurements at different joint levels in frontal and sagittal reconstructions. CD and control elbows compared using a Mann Whitney U test

	CD elbows (mm)	Control elbows (mm)	p-value
FrA	0.6	0.0	<0.0001
FrB	0.05	0.0	0.31
SagB	0.0	0.0	0.73

Figure 43 Distribution of joint incongruency measurements at FrA in CD and control elbows

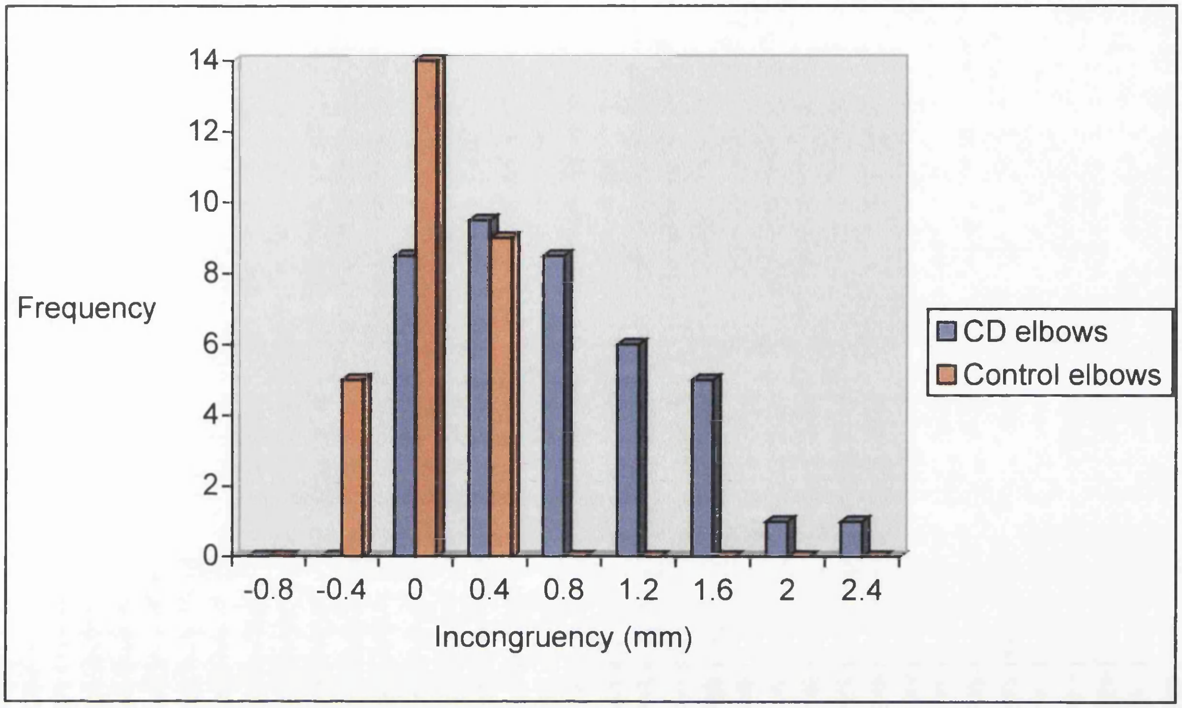

Figure 44 Analysis of variance of incongruency at different joint levels in CD and control elbows

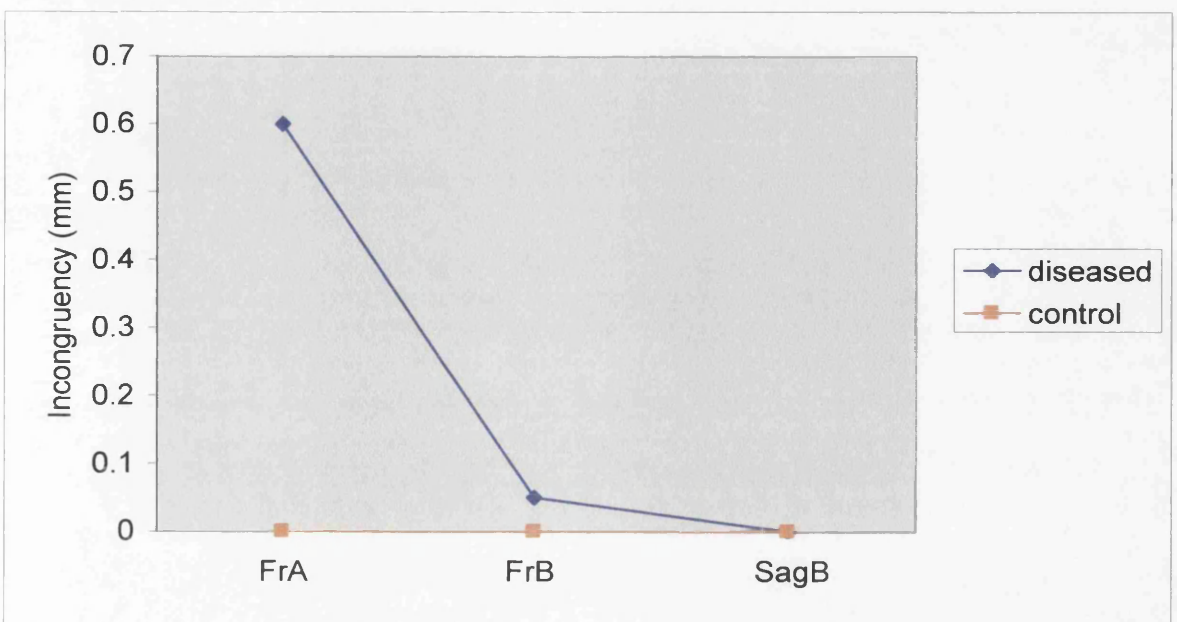

Figure 45 Box plot of joint space measurements at FrA. CD and control joint spaces compared using a Mann Whitney U Test

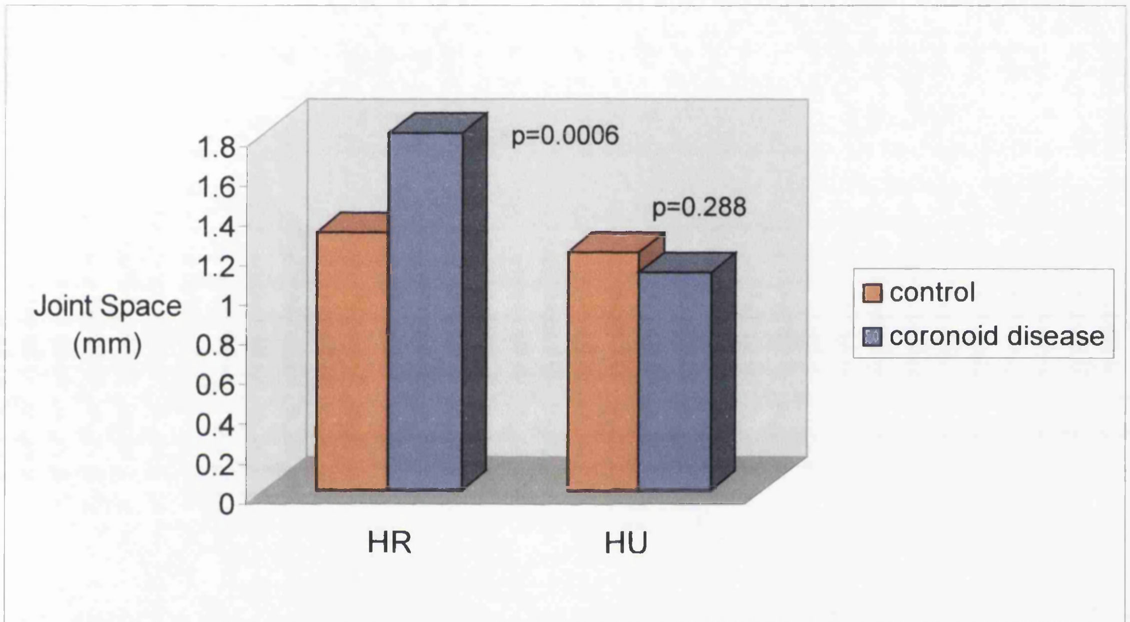

Discussion

Plain radiology is the most common form of imaging available to veterinary surgeons in the UK. However, because of its unreliability and insensitivity (Murphy and others 1998, Mason and others 2002), plain radiology is unsuitable for the investigation of subtle elbow joint incongruency in dogs suffering coronoid disease. Reconstructed CT (rCT) has been shown to be useful for the estimation of joint spaces in human elbows (Seiler and others 1995) but despite preliminary investigations (Holsworth and others 2003) its use in dogs had not been fully validated.

The normal elbows chosen for part one of this study were from Collie-type dogs, a breed not commonly affected by elbow dysplasia. Initial clinical and radiographic examination, together with the post-imaging gross examination of the joint surfaces, excluded pathology in these elbows. Examination of transverse CT images also failed to identify elbow disease. Elbows from medium and large breed dogs were selected to allow assessment of a variety of different sized elbows. Toy and small breed dogs were not included as these breeds are less likely to suffer CD (Morgan and others 2000). Evaluation of elbows from giant breed dogs would have been useful, but normal elbows from such breeds were not available for evaluation.

Elbows were scanned in pairs and in slight extension to simulate the clinical situation (de Rycke and others 2002). We used a third generation circular CT scanner for all scans. Slice thickness was set at 1.2mm and the bed increment at 1mm, the narrowest settings available for this machine, to give the most detailed images. Previous studies have employed similar protocols (de Rycke and others 2002). The effect of the make and specification of the scanner was not assessed in this study, but more variable results could be expected if less detailed scans were acquired. Conversely, modern scanners with higher specification may allow more accurate images to be obtained. Furthermore, the effect of different image analysis software packages was not investigated. Caution should be exercised in extrapolating the results of this study to different CT systems.

Since the elbow joint spaces may vary between different areas of the joint (de Rycke and others 2002), and because differences in the plane of reconstructed images may lead to variation in joint space measurements (Holsworth and others 2003), a standard transverse CT slice template was used to plan the reconstructed images in order to minimise error. This allowed rCT images to be formatted at consistent levels within the elbow. The template slice and points of reference for planning the planes of reconstructed images were easily identified in all elbows.

The results of part one of this study were analysed graphically and by using statistical calculations. Since the data were assessed with respect to equivalence between data sets, simple demonstration of nonsignificant differences was considered to be statistically inadequate (Christley and Reid 2003). Equivalence and variation between data sets is better demonstrated using graphical techniques such as Bland and Altman Plots (Bland and Altman 1986, Bland and Altman 1999). In this study, for data where the means of multiple paired points was very similar, modified plots were employed to extend the x-axis and allow easier graphical assessment of variation. Simple statistical calculations, consisting of standard deviations and Pearson correlation coefficients, were also employed in part one to further assess variation and correlations between data sets. In part two of the study, more familiar non-significant difference tests, consisting of Mann-Whitney U tests and Kruskal-Wallis tests, were used to assess differences between CD and control elbow joint incongruency.

Inter-image data indicated good agreement between rCT images of the same elbows obtained from different CT scans. This implies that minor differences in positioning of the elbows, especially minor variations in extension and rotation, have minimal effect on the rCT images and the joint space values as defined in this study. This is in part supported by an early radiographic study which indicated elbows cannot be made to appear incongruent by altering their positioning (Wind 1986a). The effects of applying larger bending or torsional stresses to the elbows during positioning were not assessed. However, it is logical to assume that such stresses could affect joint space measurements. It seems prudent to avoid stressing elbows during positioning when assessing clinical cases.

Intra-observer data also indicated good agreement between rCT images of the same elbows reviewed by a single observer on different occasions. This indicates there is minimal intra-observer variation in analysis of rCT images. In contrast, inter-observer correlation was only moderate. However, the standard deviation of the variation between paired data points for different observers was only +/- 0.22 mm (range 0 to 0.5 mm). From a clinical perspective, this implies that despite only moderate correlation, different observers can estimate joint space magnitude to an accuracy of a few tenths of a millimetre. The small variation between observers is likely to be due to an imprecise resolution of the bone contour on these rCT images leading to a degree of subjectivity in accurately measuring joint spaces. It is possible that more sophisticated CT scanners and software could reduce this variation. With our system, the use of a single observer to analyse data for subsequent parts of the study helped to minimise errors.

Comparison of rCT images with frozen sections demonstrated good agreement, both visually and using joint space measurements. This indicates that rCT can accurately image elbow joint spaces. Visually, rCT images did exhibit slight differences when compared to the corresponding frozen sections. This discrepancy is likely to be due to the formatting of rCT images in slightly different planes to the frozen sections. The joint space measurements were unaffected by this discrepancy.

In the final section of part one of this project, the ability of rCT to accurately measure joint surface incongruency was assessed. The model allowed accurate movement of the proximal radius in a distal direction which induced a radioulnar and humeroradial incongreuncy. Changes in the humeroradial joint space were confirmed using the humeral and radial radiolucent markers. The FrHR and SagHR measurements agreed well with the known induced incongruencies. This provided further evidence that rCT can be used to accurately measure joint spaces on both frontal and sagittal plane reconstructions and that these measurements are valid in both normal and incongruent joints. During radial shortening, distal movement of the humeral condyle was prevented by the presence of the medial coronoid process. JI was calculated from FrHR and FrHU measurements, and was shown to agree closely with the known induced incongruencies. This indicates that frontal plane rCT can be used to accurately measure JI.

The lack of control of small cranial movements of the humerus during radial shortening was unexpected. The reason for these movements was unclear. Incongruency secondary to cranial displacement of the humerus with respect to the trochlear notch has been reported in association with FCP (Boulay 1998), though only a single case was described. It is possible that the model in this study was inducing a similar incongruency. Alternatively, the cranial movement of the humerus may have been artefactual due to instability of the joint secondary to sectioning of the lateral collateral ligament.

Since these cranial movements of the humerus implicitly affected HU measurements on sagittal reconstructions, it was felt that this model was unreliable for direct assessment of the accuracy of sagittal plane rCT images for measurement of JI. However, data from earlier parts of this study demonstrated that sagittal plane rCT can be used to accurately and reliably measure both HR and HU joint spaces in normal elbows. Furthermore, the close agreement between SagHR values and induced incongruency in this part of the study indicates that sagittal rCT can be used to measure increases in joint spaces in incongruent elbows. Taken together, these data suggest that sagittal rCT can be used to measure JI, as defined by the difference between HR and HU, in clinical cases. This technique was subsequently employed in part two of the study.

As the induced incongruency was increased, a slight difference (range 0.2 to 0.7mm) of the rCT measured joint spaces as compared to induced incongruency was noted. The reason for this variation is unclear, but could be due to small cranial or torsional movements of the humeral condyle during radial shortening. Alternatively, it may be that rCT images obtained and analysed using this protocol may underestimate joint spaces as incongruency increases. Further studies utilising a more sophisticated model would be required to test this hypothesis. From a clinical standpoint, larger radioulnar incongruencies of 3-4 mm appear to be rarely encountered, and any smaller errors incurred when measuring smaller incongruencies are unlikely to be of clinical significance. Furthermore, rCT was able to accurately identify incongruency in all elbows in this study after just 1mm of radial shortening, implying the technique is highly sensitive for the detection of even small incongruencies.

This data indicated that direct measurement of radioulnar JI (JIRU) from sagittal rCTs was unreliable. Preliminary work by Holsworth and others (2003) had indicated that such direct measurements were possible, but were prone to variation. Only measurements from specific rCT planes were found to be reliable and geometric image analysis was required to decrease errors associated with subjectivity. The technique described in this study of calculating JI from HR and HU measurements is simple and reliable. However, since the technique uses the humeral condyle as a reference, the values obtained for JI are reliant on the integrity of the humeral condyle. Since CD is a developmental condition (Olsson 1983, Read and others 1990), it is possible that changes in joint loading secondary to the proposed incongruency could affect the development and eventual surface contour of the humeral condyle. It has been shown that the femoral trochlea does not develop appropriately in cases of developmental patellar luxation due to a lack of loading between the patella and the trochlear groove (Hulse 1993). If the humeral condyle is maldeveloped, joint space measurements and hence radioulnar JI estimations could be altered. Further work is required to investigate these possibilities and to investigate the clinical significance of any changes in humeral condyle morphology.

Joint spaces in this study were measured as bone-to-bone width, visualised using a bone window. Due to the inability of rCT to accurately image articular cartilage, it is not possible to gain further information from clinical cases on structures occupying the bone-to-bone joint space. Subjectively, high quality resolution of articular cartilage could not be achieved, even on a soft tissue window. Alternative imaging such as MRI (Snaps and others 1997, Snaps and others 1998, Snaps and others 1999) or CT arthrography (Singson and others 1986, Holland and others 1994) may better image the intra-articular structures and give further information on cartilage thickness. However, further work is needed to validate these techniques with respect to cartilage imaging in canine elbows.

Part two of this study necessitated categorization of elbows into CD and control groups. Diagnosis of CD is challenging when based on plain radiographs alone. The medial coronoid process is difficult to visualise (Robbins 1980, Henry 1984) and a presumptive diagnosis is often made indirectly based on the radiographic presence of osteophytes in the elbows of young dogs of typically affected breeds (Bennett and others 1981, Denny and Gibbs 1980). However, a proportion of dogs with CD do not show typical radiographic signs of osteoarthritis (Meyer-Lindenberg and others 2002a). In addition to the standard mediolateral and craniocaudal views, various special views have been proposed to improve visualisation of the medial coronoid process. Miyabayashi and others (1995) evaluated the use of 15-30^{o} craniolateral-caudomedial oblique views. The cranial border of the medial coronoid process was found to be best evaluated with a craniolateral-15^{o}-caudomedial oblique view. Wosar and others (1999) investigated five different radiographic projections and again concluded that the craniolateral-15^{o}-caudomedial oblique was the most sensitive for detection of FCP. More recently, Haudiquet and others (2001) proposed a distomedial-proximolateral oblique (DiMPLO) view and concluded this was more reliable than standard mediolateral and craniocaudal projections for the detection of coronoid fragmentation. However, all these oblique views can be difficult to interpret and frequently add little to the diagnosis of the disease.

Standard transverse CT images allow excellent visualisation of the coronoid process without superimposition of adjacent bony structures (Rovesti and others 2002, Reichle and others 2000) and have been shown to have high sensitivity and specificity for the diagnosis of FCP (Carpenter and others 1993). Anecdotally, CT appears to have an even higher sensitivity and specificity for the detection of subtle abnormalities of the shape and contour of the medial coronoid process which could indicate the presence of 'coronoid disease' rather than bony fragmentation of the coronoid process. The combination of radiographic and CT evaluation in this study, together with clinical information, allowed a thorough assessment of each joint prior to allocation of elbows to CD or control groups. The exclusion of cases in which the diagnosis was uncertain further improved the accuracy of diagnosis. Further assessment of elbows by arthrotomy or arthroscopy may have allowed more detailed examination of the coronoid process (Read and others

1990, Van Ryssen and van Bree 1997) and may have improved the identification of case and control elbows. In particular, the possibility of control elbows having normal radiographic and CT appearance but significant cartilage pathology could have been excluded. However, this information was not available for conservatively treated or control elbows in this retrospective study. Invasive assessment of age matched control elbows would be difficult to justify in these client owned dogs. In part 1 of this study, dissection of cadaver elbows at the end of the study allowed inspection of the cartilage of the medial compartment of the joint to exclude pathology.

For part 2 of this study, elbows for which CT scans and radiographs had been obtained at GUVS over a three year period were used. Mostly, these were dogs suspected of suffering CD, although a proportion had been scanned to check for other conditions such as incomplete ossification of the humeral condyle (IOHC). The control elbows in this study consisted of the contralateral elbow of dogs with unilateral CD, and dogs being negatively screened for IOHC. Since the median age of these dogs at the time of scanning was 12 months and CD is a developmental condition, it can be assumed that normal elbows at this time were unlikely to develop CD in the future (Olsson 1983, Read and others 1990). Because many dogs being assessed for CD in this retrospective study had only distal elbow joint CT scans, no information was available regarding the anconeus and proximal humeroulnar articulation. This information may have been useful for evaluation of the shape of the trochlear notch and the 'fit' of the humeral condyle to this shape. A future study with longer scan lengths would be useful to further assess this region of the joint.

The age of dogs diagnosed with CD in this study was typical (Bennett and others 1981, Read and others 1990). Labrador and Golden Retrievers were the most commonly affected breeds. The lower number of breeds such as Bernese Mountain Dogs, Rottweilers and Mastiffs which have been reported to be commonly affected with CD (Grøndalen 1979, Denny and Gibbs 1980, Ubbink and others 1999) is likely to reflect a lower overall number of these breeds in the local dog population rather than indicating a decrease in the prevalence of CD in certain breeds. A further study incorporating a standardised control population would be required to fully assess this.

CD dogs in this study were slightly heavier than controls. Accurate weight matching of case and control dogs is difficult in a retrospective study. However, since we evaluated JI, defined as the difference between HR and HU joint space measurements, the effect of this weight discrepancy is limited. When control dogs were evaluated as a separate group, no relationship between weight and JI was identified. Furthermore, although statistically significant, the absolute difference in the median weights of case and control dogs was only 3 kg. This is unlikely to be of clinical significance.

A clear protocol to determine incongruency based on joint space measurements from rCT images has not been previously described in the literature. To allow consistent evaluation of different areas of the elbow joint, a system of planning the planes of reconstructed images was based on a transverse CT slice template was devised. As in part 1, the template slice through the apex of the coronoid process and the points of reference for planning reconstructions were easily identified in all cases.

To minimise variation, the elbows in part two of the study were positioned in a consistent fashion for radiography and CT scanning. As demonstrated in part one of the study, small variations in the degree of extension or rotation of the elbows do not influence joint space measurements. To eliminate inter-observer variation, the scans in part two were reviewed by a single experienced observer. Narrow slice thickness and small bed increments ensured high quality images were obtained (Stickle and Hathcock 1993).

This study demonstrates that radioulnar incongruency exists at the apex of the coronoid process in CD elbows although no incongruency exists at the base. This is in contrast to a previous report which suggested that radioulnar incongruency consists of a simple undergrowth of the radius (Wind 1982). The observation of an apical radioulnar incongruency supports the hypothesis that joint surface incongruency is involved in the pathogenesis of CD in dogs. This incongruency could lead to increased loading of the medial coronoid process which could then lead to cartilage erosions of the medial compartment of the elbow joint (van Ryssen and van Bree 1997, Schulz and Krotscheck 2003) or fracture of the coronoid process (Guthrie and others 1992b). The precise mechanism of development of the incongruency cannot be determined from this cross-sectional study.

Direct comparison of HR and HU measurements at the coronoid apex demonstrated an increased HR joint space in CD elbows. This could be due to an undergrowth of the cranial portion of the radial head, an overgrowth of the apical portion of the coronoid process or a malformation of the distal humerus. The theory of coronoid overgrowth is supported by another study which noted a decreased arc of curvature of the apical portion of the coronoid in Rottweilers, a breed commonly affected by FCP, when compared with Greyhounds, a breed 'resistant' to the development of CD (Collins and others 2001). Alternatively, it is possible that a transient undergrowth of the radius relative to the ulna occurred at an earlier stage in the disease. Following gross changes in joint surface morphology due to changes in transarticular loading, the radius could have then 'caught up' with the ulna, re-establishing some contact with the humerus at the level of the coronoid base but leaving the joint surfaces ultimately incongruent.

This theory could also explain why not all CD elbows in this study had measurable incongruency at the time of scanning. A transient incongruency may have resolved by the time of referral, although secondary pathology such as fragmentation of the coronoid process, cartilage erosions in the medial compartment of the elbow and osteoarthritis persisted. The possibility of a transient incongruency could be further investigated with a linear cohort study involving sequential scans of susceptible animals over the course of disease development. Detailed imaging of the articular surface in such a study, possibly using techniques such as MRI as well as CT, may provide additional information regarding the formation of incongruencies and the pathogenesis of the disease.

A variety of osteotomies have been described to address incongruencies associated with CD (Thompson and Robbins 1995, Ness 1998, Hulse 2002). These techniques have been reported to give good clinical results with few complications. However, other authors have reported significant postoperative morbidity following such procedures (Beale 2001, Meyer-Lindenberg and others 2001). Controlled large-scale studies evaluating the outcome of clinical cases following osteotomies are lacking. Our data have shown that incongruency is not present in all dogs at the time of diagnosis, implying that osteotomy for every dog presenting with CD is unjustified. Furthermore, the data suggest that if incongruency is present at the time of diagnosis, it is likely to be present only at the apex of the coronoid. Correction of incongruency at the level of the coronoid apex may induce a subsequent incongruency at the level of the coronoid base, which could lead to further problems. Alternative techniques such as subtotal coronoidectomy (Fitzpatrick and O'Riordan 2004) may be beneficial since incongruency at the level of the coronoid apex can be addressed without affecting the elbow articulation at the level of the coronoid base. However, despite encouraging preliminary data, biomechanical studies and long term objective follow-up of clinical cases following coronoidectomy have not been performed, and further evaluation of the procedure is required.

Rather than addressing underlying incongruency, some authors have suggested that osteotomy may represent a potential treatment for CD by favourably altering transarticular loading and pressure within the joint (Mason and others 2003). Alternatively, osteotomy may have other advantageous effects such as relieving intra-osseous pressure and contributing to long term analgesia. These proposals are based on the success of high tibial osteotomy for the treatment of human unicompartmental knee osteoarthritis (Nagel and others 1996). For the canine elbow, a humeral osteotomy has been developed (Mason and others 2003, Fujita and others 2003): subsequent to observations that cartilage loss appears to be predominantly centred on the medial aspect of the joint in elbow dysplasia, the authors proposed that shifting transarticular loading towards the lateral aspect of the elbow may be beneficial. Cadaver studies confirmed that this can be achieved by using either humeral wedge or humeral slide osteotomies (Mason and others 2003). However, the osteotomies also induced a decrease in the area of the proximal radial weight-bearing surface, and the longer term implications of this are unknown at the present time. The techniques have been applied to a limited number of clinical cases following arthroscopic confirmation of healthy cartilage within the lateral compartment of the elbow (Schulz KS 2004, personal communication). Unpublished results so far indicate a favourable response to surgery (as measured by force-plate gait analysis) but severe complications have been encountered in some cases. Further investigation is required into the long-term biomechanical and physiological effects of these osteotomies, and studies to document outcomes in clinical cases are necessary before recommendations can be made regarding these procedures.

As a result of the dogs in this study being heavily sedated or anaesthetised for scanning, the effect of weight bearing and muscular forces on the joint could not be evaluated. It is likely that these forces exert a profound effect on the elbow articulation and that joint space and joint incongruency measurements may be altered (Mason and others 2002). Furthermore, measurements may be altered as the joint moves through the normal gait cycle. Other techniques incorporating weight-bearing imaging would be required to address these considerations.

The data in this study does not directly consider transarticular pressures. It is likely that the incongruency identified in this study will lead to focal increases in joint loading and pressure, and this could then lead to the development of classical lesions such as cartilage erosions and medial coronoid process fragmentation (Hak and others 1998, Preston and others 2001, Mason and others 2003). Direct measurement of transarticular pressures in clinical patients and live control animals would be extremely difficult.

Conclusions

Part one of this study demonstrated that rCT does accurately reflect the joint surface morphology of the canine elbow joint. Images, and subsequent joint space measurements, can be reliably and repeatably obtained with low intra- and inter-observer variation, accurate to a few tenths of a millimetre. Furthermore, rCT can be used to accurately measure changes in joint spaces and joint incongruency using either frontal or sagittal plane images.

Part two of this study demonstrated that radioulnar incongruency does exist at the level of the coronoid apex in elbows affected by coronoid disease, but that no incongruency is apparent at the level of the coronoid base. This association supports the theory that joint surface incongruency is involved in the pathogenesis of coronoid disease in dogs. However, incongruency was not identified in all affected elbows, and thus the routine use of osteotomies to treat these cases should be reconsidered. Further investigation is required to establish the precise mechanism of formation of incongruency in affected elbows, and to evaluate the possibility of a transient incongruency.

References

Bardet JF and Bureau S (1996). Fragmentation of the coronoid process in dogs. A case-control study of 83 elbows treated by shortening osteotomy of the proximal ulna. *Pratique Medicale et Chirurgicale de L'Animal de Compagnie* **31**, 451-463

Bardet JF (1997). Arthroscopy of the elbow in dogs. Part II: The cranial portals in the diagnosis and treatment of the lesions of the coronoid process. *Veterinary and Comparative Orthopaedics and Traumatology* **10**, 60-66

Bennett D, Duff SRI, Kene RO and Lee R (1981). Osteochondritis dissecans and fragmentation of the coronoid process in the elbow joint of the dog. *Veterinary Record* **109**, 329-336

Beale B (2001). Treatment of fragmented coronoid process. Proceedings of BSAVA satellite meeting on canine osteoarthritis, Birmingham, UK

Beale B (2002). Arthroscopic investigation of the elbow joint. Proceedings of the 1st University of Liverpool Basic Canine Arthroscopy Meeting, Liverpool, UK

Bland MJ and Altman DG (1986). Statistical methods for assessing agreement between two methods of clinical measurement. *Lancet* **347**, 307-310

Bland MJ and Altman DG (1999). Measuring agreement in method comparison studies. *Statistical Methods in Medical Research* **8**, 135-160

Bojrab MJ (1981). Fragmented coronoid process. In: Pathophysiology in Small Animal Surgery. Ed: Bojrab MJ, Lea and Febinger, Philadelphia, USA. p529-532

Boulay JP (1998). Fragmented medial coronoid process of the ulna in the dog. *Veterinary Clinics of North America (Small Animal Practice)* **28**, 51-74

Bouck GR, Miller CW and Taves CL (1995). A comparison of surgical and medical treatment of fragmented coronoid process and osteochondritis dissecans of the canine elbow. *Veterinary and Comparative Orthopaedics and Traumatology* **8**, 177-183

Braden TD, Stickle RL, Dejardin LM, Mostosky UV (1994). The use of computed tomography in fragmented coronoid disease: a case report. *Veterinary and Comparative Orthopaedics and Traumatology* **7**, 40-44

Cameron HU, Botsford DJ and Park YS (1997). Prognostic factors in the outcome of supracondylar femoral osteotomy for lateral compartment osteoarthritis of the knee. *Canadian Journal of Surgery* **40**, 114-118

Carpenter LG, Schwarz PD, Lowry JE, Park RD and Steyn PF (1993). Comparison of radiologic imaging techniques for diagnosis of fragmented medial coronoid process of the cubital joints in dogs. *Journal of the American Veterinary Medical Association* **203**, 78-83

Christley RM and Reid SW (2003). No significant difference: use of statistical methods for testing equivalence in clinical veterinary literature. *Journal of the American Veterinary Medical Association* **222**, 433-437

Collins KE, Cross AR, Lewis DD, Zapata JL, Goett SD, Newell SM and Rapoff AJ (2001). Comparison of the radius of curvature of the ulnar trochlear notch of Rottweilers and Greyhounds. *American Journal of Veterinary Research* **62**, 968-973

Conzemius M (2004). Postoperative rehabilitation and exercise. Proceedings of the AO-ASIF Advanced Techniques in Small Animal Fracture Management meeting, Columbus, Ohio, USA

Corley EA and Carlson WD (1965). Radiographic, genetic, and pathological aspects of elbow dysplasia. *Journal of the American Veterinary Medical Association* **147**, 1651-1655

Crouch DT, Cook JL, Lewis DD, Kreeger JM and Tomlinson JL (2000). The presence of collagen types II and X in medial coronoid processes of 21 dogs. *Veterinary and Comparative Orthopaedics and Traumatology* **13**, 178-184

Denny HR and Gibb C (1980). The surgical treatment of osteochondritis dissecans and ununited coronoid process in the canine elbow joint. *Journal of Small Animal Practice* **21**, 323-326

Edelson G, Kunos CA, Vigder F and Obed E (2001). Bony changes at the lateral epicondyle of possible significance in tennis elbows syndrome. *Journal of Shoulder and Elbow Surgery* **10**, 158-163

Eckstein F, Lohe F, Muller-Gerbl M, Steinlechner M and Putz R (1994). Stress distribution in the trochlear notch. A model of bicentric load transmission through joints. *Journal of Bone and Joint Surgery (British)* **76**, 647-653

De Rycke LM, Gielen IM, van Bree H and Simoens PJ (2002). Computed tomography of the elbow joint in clinically normal dogs. *American Journal of Veterinary Research* **63**, 1400-1407

Edelson G, Kunos CA, Vidger F and Obed E (2001). Bony changes at the lateral epicondyle of possible significance in tennis elbow syndrome. *Journal of Shoulder and Elbow Surgery* **10**, 158-163

Fitzpatrick MN and Reuter R (2004). Histopathology of cartilage and subchondral bone following subtotal coronoidectomy (SCO) for the treatment of fragmented medial coronoid process. Proceedings of the 47th BSAVA congress clinical research abstracts, Birmingham p586

Fitzpatrick MN and O'Riordan J (2004). Clinical and radiographic assessment of 83 cases of subtotal coronoidectomy (SCO) for treatment of fragmented medial coronoid process. Proceedings of the 47th BSAVA congress clinical research abstracts, Birmingham p594

Franklin PD, Dunlop RW, Whitelaw G, Jaques E Jr, Blickman JG and Shapiro JH (1988). Computed tomography of the normal and traumatised elbow. *Journal of Computed Assisted Tomography* **12**, 817-823

Fujita Y, Schulz KS, Mason DR, Kass PH and Stover SM (2003). Effect of humeral osteotomy on joint surface contact in canine elbow joints. *American Journal of Veterinary Research* **64**, 506-511

Gielen I and van Bree H (2003). Computed tomography in small animals. Part 2. Clinical applications. *Vlaams Diergeneeskundig Tijdschrift* **72**, 168-179

Grøndalen J (1976). Diseases in the shoulder and elbow joints of young rapidly growing dogs. *Norsk Veterinaer Tidsskrift* **88**, 309-316

Grøndalen J (1979). Arthrosis with special reference to the elbow joint of young, rapidly growing dogs (II). Occurrence, clinical and radiographic findings. *Nordisk Veterinaermedicin* **31**, 69-75

Grøndalen J and Grøndalen T (1981). Arthrosis in the elbow joint of young rapidly growing dogs (V). A pathoanatomical investigation. *Nordisk Veterinaermedicin* **33**, 1-16

Grøndalen J (1982). Arthrosis in the elbow joint of young rapidly growing dogs. *Nordisk Veterinaermedicin* **34**, 76-82

Guthrie S and Pidduck HG (1990). Heritability of elbow osteochondrosis within a closed population of dogs. *Journal of Small Animal Practice* **31**, 93-96

Guthrie S, Plummer JM and Vaughan LC (1992a). Post natal development of the canine elbow joint: a light and electron microscopic study. *Research in Veterinary Science* **52**, 67-71

Guthrie S, Plummer JM and Vaughan LC (1992b). Aetiopathogenesis of canine elbow osteochondrosis: a study of loose fragments removed at arthrotomy. *Research in Veterinary Science* **52**, 284-291

Hak DJ, Hamel AJ, Bay BK and others (1998). Consequences of transverse acetabular fracture malreduction on load transfer across the hip joint. *Journal of Orthopaedic Trauma* **12**, 90-100

Hare WCD (1961). The ages at which the centres of ossification appear roentgenographically in the limb bones of the dog. *American Journal of Veterinary Research* **22**, 825-835

Hathcock JT and Stickle RL (1993). Principles and concepts of computed tomography. *Veterinary Clinics of North America (Small Animal Practice)* **23**, 399-415

Haudiquet PR, Marcellin-Little DJ, Stebbins ME (2001). Use of the distomedial-proximolateral oblique radiographic view of the elbow joint for examination of the medial coronoid process in dogs. *American Journal of Veterinary Research* **63**, 1000-1005

Henry WB (1984). Radiographic diagnosis and surgical management of fragmented medial coronoid process in dogs. *Journal of the American Veterinary Medical Association* **184**, 799-805

Holland P, Davies AM and Cassar-Pullicino VN (1994). Computed tomographic arthrography in the assessment of osteochondritis dissecans of the elbow. *Clinical Radiology* **49**, 231-235

Holsworth IG, Wisner E, Scherrer WE, Kass P, Pooya H, Schulz KS (2003). Accuracy of computerised tomographic evaluation of canine radio-ulnar incongruency in vitro. Proceedings of the 30th Annual Meeting of the Veterinary Orthopaedic Association, Steamboat Springs, Colorado, USA p37

Huibregste BA, Johnson AL, Muhlbauer MC and Pijanowski GJ (1994). The effect of treatment of fragmented coronoid process on the development of osteoarthritis of the elbow. *Journal of the American Animal Hospital Association* **30**, 190-195

Hulse DA (1993). Medial patellar luxation in the dog. In: Disease Mechanisms in Small Animal Surgery, 2nd Edition. Ed: Bojrab MJ. Lippincott, Williams and Wilkins, Pennsylvania, USA p808-817

Hulse D (2002). Treatment of canine elbow dysplasia. Proceedings of the 1st University of Liverpool Basic Canine Arthroscopy Meeting, Liverpool, UK

Kealy RD, Lawler DF, Ballam JM, Lust G, Biery DN, Smith GK and Mantz S (2000). Evaluation of the effect of limited food consumption on radiographic evidence of osteoarthritis in dogs. *Journal of the American Veterinary Medical Association* **217**, 1678-1680

Korbel J, Wilcken R and Huskamp B (2001). Computed tomographic examination of the canine elbow joint. *Kleintierpraxis* **46**, 325-331

Llinas A, McKellop HA, Marshall GJ and others (1999). Healing and remodelling of articular incongruities in a rabbit fracture model. *Journal of Bone and Joint Surgery (American)* **75**, 1508-1523

MacPherson GC, Lewis DD, Johnson KA, Allen GS, Yovich JC (1992). Fragmented coronoid process associated with premature distal radial physeal closure in four dogs. *Veterinary and Comparative Orthopaedics and Traumatology* **5**, 93-99

Maierl J, Hecht S, Botscher P, Matis U and Liebich HG (2000). New aspects of the functional anatomy of the canine elbow joint. Proceedings of the 10th Annual European Society of Veterinary Orthopaedics and Traumatology, Munich, Germany p90

Maki K, Liinamo AE and Ojala M (2000). Estimates of genetic parameters for hip and elbow dysplasia in Finnish Rottweilers. *Journal of Animal Science* **78**, 1141-1148

Maki K, Groen AF, Liinamo AE and Ojala M (2002). Genetic variances, trends and modes of inheritance for hip and elbow dysplasia in Finnish dog populations. *Animal Science* **75**, 197-207

Mason DR, Schulz KS, Samii VF, Fujita Y, Hornoff WJ, Herrgesell EJ, Long CD, Morgan JP and Kass PH (2002). Sensitivity of radiographic evaluation of radioulnar incongruence in the dog in vitro. *Veterinary Surgery* **31**, 125-132

Mason DR, Schulz KS, Yukihiro Fujita, Kass PH and Stover SM (2003). Reduction of load on the proximal articular surface of the ulna after humeral wedge and humeral slide osteotomies. Proceedings of the 30th Annual Meeting of the Veterinary Orthopaedic Association, Steamboat Springs, Colorado, USA p55

Meyer-Lindenberg A, Fehr M and Nolte I (2001). Short and long term results after surgical treatment of an ununited anconeal process in the dog. *Veterinary and Comparative Orthopaedics and Traumatology* **14**, 101-110

Meyer-Lindenberg A, Langhann A, Fehr M and Nolte I (2002a). Prevalence of fragmented medial coronoid process of the ulna in lame adult dogs. *Veterinary Record* **151**, 230-234

Meyer-Lindenberg A, Staszyk C, Gasse H, Fehr M and Nolte I (2002b). Caudomedial approach for removal of an ununited anconeal process and assessment of the medial coronoid process of the ulna. *Journal of Veterinary Medicine - Series A* **49**, 277-280

Meyer-Lindenberg A, Heinen V, Hewicker-Trautwein M and Nolte I (2004a). Occurrence of calcified bodies in the flexor tendons arising from the medial humeral epicondyle as a cause of lameness in dogs and results of treatment. Proceedings of the 47th BSAVA congress clinical research abstracts, Birmingham p587

Meyer-Lindenberg A and Heinen V (2004b). Therapy and results of chondromalacia like lesions and cartilage abrasions in the canine elbow joint. Proceedings of the 47th BSAVA congress clinical research abstracts, Birmingham p584

Miyabayashi T, Takiguchi M and Schrader SC (1995). Radiographic anatomy of the medial coronoid process of dogs. *Journal of the American Animal Hospital Association* **31**, 125-132

Morgan JP, Wind AP and Davidson J (1999). Bone dysplasias in the Labrador Retriever: a radiographic study. *Journal of the American Animal Hospital Association* **35**, 332-340

Morgan JP, Wind AP and Davidson J (2000). Elbow dysplasia. In: Hereditary Bone and Joint Diseases in the Dog. Schlutersche, Hannover, Germany, p41-68

Murphy ST, Lewis DD, Shiroma JT and others (1998). Effect of radiographic positioning on interpretation of cubital joint congruity in dogs. *American Journal of Veterinary Research* **11**, 1351-1357

Nagel A, Insall JN and Scuderi GR (1996). Proximal tibial osteotomy. A subjective outcome study. *Journal of Bone and Joint Surgery (American)* **78**, 1353-1358

Ness M (1998). Treatment of fragmented coronoid process in young dogs by proximal ulnar osteotomy. *Journal of Small Animal Practice* **39**, 15-18

Olsson SE (1974). A new type of elbow dysplasia in the dog. A preliminary report. *Svensk Veterinartidning* **5**, 152-157

Olsson SE (1975). Lameness in the dog. *Proceedings of the American Animal Hospital Association Annual Meeting* **42**, 363

Olsson SE (1983). The early diagnosis of fragmented coronoid process and osteochondritis dissecans of the canine elbow. *Journal of the American Animal Hospital Association* **19**, 616-626

Piermattei D and Johnson K (2004). Medial approach to the radius. In: An Atlas of Surgical Approaches to the Bones and Joints of the Dog and Cat, 4th Edition. Eds: Piermattei D and Johnson K. Saunders, Philadelphia, USA p246-249

Potter HG (2000). Imaging of posttraumatic and soft tissue dysfunction of the elbow. *Clinical Orthopaedics and Related Research* **370**, 9-18

Preston CA, Schulz KS and Kass PH (2000). In vitro determination of contact areas in the normal elbow joint of dogs. *American Journal of Veterinary Research* **61**, 1315-1321

Preston CA, Schulz KS, Taylor KT, Kass PH, Hagan CE and Stover SM (2001). In vitro experimental study of the effect of radial shortening and ulnar ostectomy on contact patterns in the elbow joint of dogs. *American Journal of Veterinary Research* **62**, 1548-1556

Read R (1987). Fragmented coronoid process in the Rottweiler – a review of 35 cases. *Australian Veterinary Practitioner* **17**, 140-141

Read RA, Armstrong SJ, O'Keefe JD and Eger CE (1990). Fragmentation of the medial coronoid process of the ulna in dogs: a study of 109 cases. *Journal of Small Animal Practice* **31**, 330-334

Rees JL, Price AJ, Lynskey TG, Svard UC, Dodd CA and Murray DW (2001). Medial unicompartmental arthroplasty after failed high tibial osteotomy. *Journal of Bone and Joint Surgery (British)* **83**, 1034-1036

Reichle JK, Park RD and Bahr AM (2000). Computed tomographic findings of dogs with cubital joint lameness. *Veterinary Radiology and Ultrasound* **41**, 125-130

Ring D, Jupiter JB and Zilberfarb J (2002). Posterior dislocation of the elbow with fractures of the radial head and coronoid. *Journal of Bone and Joint Surgery (American)* **84**, 547-551

Robbins GM (1980). Some aspects of the radiographic examination of the canine elbow joint. *Journal of Small Animal Practice* **21**, 417-428

Rovesti GL, Biasibetti M, Schumacher A and Fabiani M (2002). The use of computed tomography in the diagnostic protocol of the elbow in the dog: 24 joints. *Veterinary and Comparative Orthopaedics and Traumatology* **15**, 35-43

Schulz KS (2003). Elbow joint contact and critical loading. *Proceedings of the BVOA Spring Meeting, Birmingham* p4-7

Schulz KS and Krotscheck U (2003). Canine elbow dysplasia. In: A Textbook of Small Animal Surgery, 3rd Edition. Ed: Slatter D. Saunders, Philadelphia, USA 1927-1952

Seiler JG, Parker LM, Chamberland PD, Sherbourne GM and Carpenter WA (1995). The distal biceps tendon. Two potential mechanisms involved in its rupture: arterial supply and mechanical impingement. *Journal of Shoulder and Elbow Surgery* **4**, 149-156

Singson RD, Feldman F and Rosenberg ZS (1986). Elbow joint: assessment with double contrast CT arthrography. *Radiology* **160**, 167-173

Snaps FR, Ballingrad MH, Saunders JH, Park RD and Dondelinger RF (1997). Comparison of radiography, magnetic resonance imaging and surgical findings in dogs with elbow dysplasia. *American Journal of Veterinary Research* **58**, 1367-1370

Snaps FR, Saunders JH, Park RD, Daenen B, Ballingrad MH, and Dondelinger RF (1998). Comparison of spin echo, gradient echo and fat saturation magnetic resonance imaging sequences for imaging the canine elbow. *Veterinary Radiology and Ultrasound* **39**, 518-523

Snaps FR, Park RD, Saunders JH, Ballingrad MH, and Dondelinger RF (1999). Magnetic resonance arthrography of the cubital joint in dogs affected with fragmented medial coronoid process. *American Journal of Veterinary Research* **60**, 190-193

Stickle RL and Hathcock JT (1993). Interpretation of computed tomographic images. *Veterinary Clinics of North America (Small Animal Practice)* **23**, 417-435

Theyse LFH, Hazewinkel HAW and van den Brom WE (2000). Force plate analyses before and after surgical treatment of unilateral fragmented coronoid process. *Veterinary and Comparative Orthopaedics and Traumatology* **13**, 135-140

Thompson MJ and Robbins GM (1995). Osteochondrosis of the elbow: a new approach to treatment. *Australian Veterinary Journal* **72**, 375-378

Tirgari M (1974). Clinical, radiographic and pathological aspects of arthritis of the elbow joint in dogs. *Journal of Small Animal Practice* **15**, 671-679

Tirgari M (1980). Clinical, radiographic and pathological aspects of ununited medial coronoid process of the elbow joints of dogs. *Journal of Small Animal Practice* **21**, 595-608

Ubbink GJ, Hazewinkel HA, Broek J and van Rothuizen J (1999). Familial clustering and risk analysis for fragmented coronoid process and elbow joint incongruity in Bernese Mountain Dogs in the Netherlands. *American Journal of Veterinary Research* **60**, 1082-1087

Van Ryssen B and Van Bree H (1997). Arthroscopic findings in 100 dogs with elbow lameness. *Veterinary Record* **140**, 360-362

Viehmann B, Waibl H and Brunnberg L (1999). Computer assisted interpretation of radiographs for elbow dysplasia in dogs (I). Trochlear incisure of the ulna. *Kleintierpraxis* **44**, 595-606

Walker TM (1998). A redefined type of elbow dysplasia in the dog – two cases. Canadian Veterinary Journal 39, 573-575

Webber KL and Morrey BF (1999). Osteoid osteoma of the elbow: a diagnostic challenge. *Journal of Bone and Joint Surgery (American)* **81**, 1111-1119

Wind AP (1982). Incidence and appearance of fragmented coronoid process in the Bernese Mountain dog. *California Veterinarian* **6**, 19-26

Wind AP (1986a). Elbow incongruity and developmental elbow disease in the dog: Part 1. *Journal of the American Animal Hospital Association* **22**, 711-724

Wind AP (1986b). Elbow incongruity and developmental elbow disease in the dog: Part II. *Journal of the American Animal Hospital Association* **22**, 725-730

Wosar MA, Lewis DD, Neuwirth L and others (1999). Radiographic evaluation of elbow joints before and after surgery in dogs with possible fragmented medial coronoid process. *Journal of the American Veterinary Medical Association* **214**, 52-58

Yovich JC and Read RA (1994). Traumatic fracture of the medial coronoid process in two dogs. *Veterinary and Comparative Orthopaedics and Traumatology* **7**, 173-176

Appendices

Appendix 1

Joint space measurements for inter-image analysis (millimetres)

Elbow	rCT 1	rCT 2	rCT 3	Variation
	FrHR	**FrHR**	**FrHR**	
2	1	0.9	1	0.1
4	0.7	0.7	0.9	0.2
5	0.8	1	0.8	0.2
8	1	0.8	1.1	0.3
	FrHU	**FrHU**	**FrHU**	
2	0.8	0.7	0.8	0.1
4	0.8	0.8	1	0.2
5	0.8	1.1	0.8	0.3
8	1	0.9	1.1	0.2
	SagHR	**SagHR**	**SagHR**	
2	1	1.1	1.2	0.2
4	0.9	0.8	0.8	0.1
5	0.8	0.8	0.8	0
8	1.1	1	0.9	0.2
	SagHU	**SagHU**	**SagHR**	
2	1.6	1.6	1.5	0.1
4	0.9	0.8	0.9	0.1
5	0.9	0.8	0.9	0.1
8	1.1	0.9	0.8	0.3

Appendix 2

Pearson correlation coefficients for inter-image analysis

Scan comparisons	**R value**
RCT 1 vs RCT 2	0.803
RCT 2 vs RCT 3	0.696
RCT 1 vs RCT 3	0.765

Appendix 3

Joint space measurement for inter-observer analysis (millimetres)

Elbow	Observer 1	Observer 2	Difference
	FrHR	**FrHR**	
2	1	1	0
4	0.7	0.8	-0.1
5	0.8	1.3	-0.5
8	1	1.2	-0.2
	FrHU	**FrHU**	
2	0.8	0.7	0.1
4	0.8	0.8	0
5	0.8		-0.1
8	1	0.9	0.1
	SagHR	**SagHR**	
2	1	1.1	-0.1
4	0.9	1.2	-0.3
5	0.8	0.8	0
8	1.1	1.1	0
	SagHU	**SagHU**	
2	1.6	1.3	0.3
4	0.9	0.8	0.1
5	0.9	0.8	0.1
8	1.1	0.7	0.4

Appendix 4

Joint space measurements for intra-observer analysis (millimetres)

Elbow	Occasion 1	Occasion 2	Occasion 3	Variation
	FrHR	**FrHR**	**FrHR**	
2	1	0.9	1	0.1
4	0.7	0.8	0.9	0.2
5	0.8	0.8	1	0.2
8	1	0.9	0.9	0.1
	FrHU	**FrHU**	**FrHU**	
2	0.8	0.7	0.8	0.1
4	0.8	1	1	0.2
5	0.8	0.7	0.7	0.1
8	1	1	1	0
	SagHR	**SagHR**	**SagHR**	
2	1	1.1	1.4	0.4
4	0.9	0.8	0.9	0.1
5	0.8	0.8	0.8	0
8	1.1	1.1	1.1	0
	SagHU	**SagHU**	**SagHU**	
2	1.6	1.6	1.6	0
4	0.9	0.9	1	0.1
5	0.9	0.8	0.8	0.1
8	1.1	0.9	0.9	0.2

Appendix 5

Pearson correlation coefficients for intra-observer analysis

Comparisons	R value
Occasion 1 vs occasion 2	0.891
Occasion 2 vs occasion 3	0.922
Occasion 1 vs occasion 3	0.768

Appendix 6

Joint space measurements for comparison of rCT images with frozen sections (millimetres)

Elbow	rCT	Frozen sections	Difference
	FrHR	FrHR	
3	1	0.8	0.2
5	0.6	0.6	0
11	0.7	0.6	0.1
12	0.9	1	-0.1
	FrHU	FrHU	
3	1	1	0
5	0.7	0.5	0.2
11	0.8	0.7	0.1
12	0.8	0.7	0.1
	SagHR	SagHR	
2	0.7	0.6	0.1
4	0.7	0.6	0.1
6	1	1.2	-0.2
8	1.2	1.4	-0.2
	SagHU	SagHU	
2	0.8	0.6	0.2
4	0.7	0.6	0.1
6	1	1.1	-0.1
8	1.4	1.2	0.2

Appendix 7

Joint space measurements for analysis of induced incongruency (millimetres)

Elbow	Induced incongruency	FrHU	FrHR	JIFr	SagHR	JIRU
1	0	1	1.1	0.1	0.8	0.7
1	1	0.9	1.9	1	1.7	0.8
1	2	1	2.8	1.8	2.7	1.5
1	3	0.9	3.8	2.9	3.7	2.4
1	4	1.1	4.7	3.6	4.6	3.1
9	0	0.8	0.7	-0.1	0.7	0.4
9	1	0.9	1.4	0.6	1.4	0.4
9	2	0.9	2.3	1.4	2.3	1.7
9	3	0.8	3.5	2.7	3.2	1.6
9	4	0.9	4.3	3.4	4.2	2
7	0	1.1	0.9	-0.2	0.9	0.4
7	1	1.2	1.8	0.6	1.7	0.5
7	2	1	2.9	1.9	2.8	1.7
7	3	1.1	3.8	2.7	3.7	1.6
7	4	1	4.7	3.7	4.7	2.5
10	0	0.9	0.9	0	0.9	0.2
10	1	1	1.7	0.7	1.8	0.4
10	2	0.8	2.9	2.1	2.7	2
10	3	0.9	3.7	2.8	3.6	1.9
10	4	0.9	4.6	3.7	4.6	2.4

Appendix 8

Increment in FrHR, SagHR, JIFr and JIRL for induced incongruency

Induced increment	**0**	**1**	**2**	**3**	**4**
1. Increase in FrHR (iFrHR)					
Elbow 1	0	0.8	1.7	2.7	3.6
Elbow 7	0	0.9	2	2.9	3.8
Elbow 9	0	0.7	1.6	2.8	3.6
Elbow 10	0	0.8	2	2.8	3.7
Mean	0	0.8	1.825	2.8	3.675
Bland and Altman mean	0	0.9	1.91	2.9	3.84
Bland and Altman difference	0	-0.2	-0.175	-0.2	-0.325
2. Increase in SagHR (iSagHR)					
Elbow 1	0	0.9	1.9	2.9	3.8
Elbow 7	0	0.8	1.9	2.8	3.8
Elbow 9	0	0.7	1.5	2.4	3.4
Elbow 10	0	0.9	1.8	2.7	3.7
Mean	0	0.825	1.775	2.7	3.675
Bland and Altman mean	0	0.913	1.888	2.85	3.838
Bland and Altman difference	0	-0.175	-0.225	-0.3	-0.325
3. Increase in JIFr (iJIFr)					
Elbow 1	0	0.9	1.7	2.8	3.5
Elbow 7	0	0.8	2.1	2.8	3.8
Elbow 9	0	0.7	1.5	2.6	3.3
Elbow 10	0	0.7	2.1	2.8	3.7
Mean	0	0.775	1.85	2.75	3.575
Bland and Altman mean	0	0.888	1.925	2.875	3.788
Bland and Altman difference	0	-0.225	-0.15	-0.25	-0.325
4. Increase in JIRU (iJIRU)					
Elbow 1	0	0.1	0.8	1.7	2.4
Elbow 7	0	0.1	1.3	1.2	2.1
Elbow 9	0	0	1.3	1.2	1.6
Elbow 10	0	0.2	1.8	1.7	2.2
Mean	0	0.1	1.3	1.45	2.08
Bland and Altman mean	0	0.55	1.65	2.225	3.04
Bland and Altman difference	0	-0.9	-0.7	-1.55	-1.92

Appendix 9

Joint space measurements and joint incongruency values for CD and control dogs in the retrospective clinical study (millimetres)

Case no	Age	Dx	Limb	FrHR (Apex)	FrHU (Apex)	FrA JI	FrHR (Base)	FrHU (Base)	FrB JI	SagHR (Base)	SagHU (Base)	SagB JI
140077	12	cd	R	2.1	1	1.1	0.7	0.6	0.1	1.1	0.7	0.4
140650		cd	L	2.1	1	1.1	0.6	0.9	-0.3	1	0.8	0.2
140650	19	cd	R	1.7	0.8	0.9	1.3	0.7	0.6	1.1	0.8	0.3
140655	24	nad	L	0.9	1.3	-0.4	1.2	1.1	0.1	1.3	1	0.3
140677	24	nad	R	1.2	1.3	-0.1	0.7	1	-0.3	1	0.9	0.1
140765	12	cd	R	2.6	1.2	1.4	1.4	1.6	-0.2	1.1	1.1	0
140765	12	nad	L	1.4	1.2	1.2	1.3	1.3	0	1.2	1	0.1
140843	33	nad	R	0.7	1.2	-0.5	0.7	0.7	0	0.7	0.7	0
140856	8	cd	L	3.5	1.1	2.4	1.5	1.1	0.4	1.2	1.8	-0.6
141175	24	cd	R	0.9	1.6	-0.7	1.3	1.3	0	1.2	1.2	0
141367	24	nad	R	1.5	1.8	-0.3	1.3	0.9	0.4	0.9	0.7	0.2
141522	6	cd	L	2.2	1.6	0.6	1.2	1.5	-0.3	1.7	1.8	-0.1
141645	13	cd	R	1.3	1.1	0.2	1	1.6	-0.6	1.2	1.2	0
141901	12	cd	L	3.1	2	1.1	2.2	2	0.2	2.3	1.9	0.4
144187	7	cd	L	1.3	1.3	0	1	1.5	-0.5	0.6	0.7	-0.1
144231	9	nad	L	1.7	1.9	-0.2	1	0.9	0.1	0.5	0.6	-0.1
144231	9	nad	R	1.3	1.1	0.2	1.6	1.4	0.2	1.1	1.2	-0.1
144618	8	nad	L	0.7	0.7	0	0.6	0.7	-0.1	0.8	0.6	0.2
144629	19	cd	L	1.3	1	0.3	1.2	1.1	0.1	1.1	0.7	0.3
144856	7	nad	R	1.3	1.4	-0.1	0.6	0.7	-0.1	0.8	0.9	-0.1
145544	18	nad	R	0.6	0.5	0.1	0.6	0.7	-0.1	0.7	0.7	0
145544	18	nad	L	0.7	0.8	-0.1	0.6	0.9	-0.3	0.6	0.7	-0.1
200280	6	cd	L	0.9	0.9	0	1.3	1.3	0	1.6	1.2	0.4
200280	6	cd	R	2.9	1	1.9	1.1	0.9	0.2	1.2	1	0.2
200334	49	nad	R	1.1	0.8	0.3	0.7	0.8	-0.1	0.6	0.8	-0.2
200334	49	nad	L	0.9	0.9	0	0.7	1	-0.3	0.5	0.6	-0.1
200337	7	cd	L	2	1.1	0.9	1	0.9	0.1	1.9	1.9	0
200337	7	nad	R	1.4	1.1	0.3	1.2	0.9	0.3	1	0.8	0.2
200394	43	cd	L	2.1	0.6	1.5	1.2	0.8	0.4	1.4	1.9	-0.5
200394	43	cd	R	2	1.4	0.6	1.7	1.7	0	1.3	1.3	0
200609	9	cd	R	3	2.1	0.9	2	1.3	0.7	1.5	3.1	1.6
200609	9	nad	L	1	1	0	0.7	0.7	0	0.9	1	-0.1
200747	18	cd	L	1.3	0.8	0.5	0.8	0.8	0	1.2	1.1	0.1
200747	18	cd	R	0.6	0.7	-0.1	0.8	0.7	0.1	1.2	1.1	0.1
200808	9	cd	L	1.8	0.5	0.3	1.2	0.5	0.7	1.5	1.8	-0.3
200808	9	nad	R	0.9	0.7	0.2	0.8	0.6	0.2	0.7	0.8	-0.1
200828	39	cd	L	1.2	1.1	0.1	1.4	1.3	0.1	0.8	1	-0.2
200828	39	nad	R	1.7	1.5	0.2	0.7	1.1	-0.4	0.9	1.1	-0.2
200834	14	cd	L	3.1	2.2	0.9	1.4	1.3	0.1	1.4	2.6	-1.7
200834	14	cd	R	1.4	1.4	0	1	0.9	0.1	1.7	1.7	0
200856	6	nad	R	1.2	1.4	-0.2	0.9	0.9	0	1.3	1.3	0
200892	48	cd	R	1.9	1.2	0.7	1	0.9	0.1	1.1	1	0.1
200892	48	nad	L	1.3	0.9	0.4	0.9	0.8	0.1	1.1	1.2	-0.1
201087	6	nad	L	1.5	1.4	0.1	1.5	1.5	0	1	1.3	-0.3
201192	15	cd	L	1	0.8	0.2	0.8	0.7	0.1	1.5	1.4	0.1

201192	15	nad	R	1.3	1.4	-0.1	0.9	1.1	-0.1	1.5	1.4	0.1
201378	25	cd	L	1.6	1.6	0	1.1	1.3	-0.2	0.9	0.9	0
201378	25	nad	R	1.6	1.5	0.1	0.8	1.1	-0.3	1.1	0.6	0.5
201442	7	cd	R	0.9	0.7	0.2	1.1	1.1	0	1.2	1.3	-0.1
201442	12	cd	L	1.4	1.3	0.1	1.2	1.2	0	0.8	1	-0.2
201671	6	cd	L	2.1	0.9	1.2	1.5	1.6	0.1	1.8	1.6	0.2
201671	6	nad	R	1.5	1.5	0	0.8	1	-0.2	0.8	0.9	-0.1
202192	8	nad	L	1.4	1.2	0.2	1.2	1.4	-0.2	0.9	0.9	0
202192	8	nad	R	1.4	1.4	0	1.4	1.3	0.1	1	0.9	0.1
202261	8	cd	R	2.3	0.7	1.6	1.9	1.9	0	1.4	2.4	-1
202261	8	cd	L	3.3	1.6	1.7	2.7	1.6	1.1	2.9	3.9	-1
202490	8	cd	L	1.8	1.4	0.4	1.1	1.7	-0.6	2	1.7	0.3
202650	8	cd	R	1.8	1.2	0.6	1.4	1.7	-0.4	1.2	1.5	-0.3
202650	9	nad	L	1.2	1.2	0	1.2	1.3	-0.1	0.7	1.1	-0.4
202736	10	cd	R	1.1	1.1	0	0.7	1.1	-0.4	0.8	1	-0.2
202736	10	cd	L	1.3	1	0.3	1.3	1.3	0	1.4	1.6	-0.2
202758	7	cd	R	2.7	1.4	1.3	1.6	1.6	0	1.4	2	-0.6
202758	7	cd	L	1.2	0.9	0.3	1.2	1.1	0.1	1.4	2	-0.6
202899	10	cd	R	2.4	1	1.4	1.4	1.5	-0.1	1.5	1.5	0
202899	10	nad	L	1.6	1.2	0.4	1.4	0.8	0.5	1.7	1.7	0
202994	22	cd	R	1.5	0.5	1	0.7	0.8	-0.1	0.7	0.8	-0.1
202994	22	cd	L	1	1	0	0.9	0.8	0.1	0.9	0.8	0.1
203265	12	nad	R	1.3	1.2	0.1	0.6	0.5	0.1	1	1	0
203265	12	cd	L	1.1	0.6	0.5	0.7	0.9	-0.2	1	1	0
203347	11	nad	R	1.2	1	0.2	1.3	1.3	0	1.3	1.3	0
203347	11	cd	L	1.8	1.2	0.6	1.5	1.2	0.3	1.1	1.2	-1